

# Stratigraphic and structural controls on groundwater flow in an outcropping fossil fan delta: the case of Sant Llorenç del Munt range (NE Spain)

Marc Anglés<sup>1</sup> · Albert Folch<sup>2,3</sup> · Oriol Oms<sup>4</sup> · Eudald Maestro<sup>4</sup> · Josep Mas-Pla<sup>5</sup>

Received: 28 November 2016 / Accepted: 5 June 2017 / Published online: 8 July 2017  
© Springer-Verlag GmbH Germany 2017

**Abstracts** Hydrogeological models of mountain regions present the opportunity to understand the role of geological factors on groundwater resources. The effects of sedimentary facies and fracture distribution on groundwater flow and resource exploitation are studied in the ancient fan delta of Sant Llorenç de Munt (central Catalonia, Spain) by integrating geological field observations (using sequence stratigraphy methods) and hydrogeological data (pumping tests, hydrochemistry and environmental isotopes). A comprehensive analysis of data portrays the massif as a single unit, constituted by different compartments determined by specific layers and sets of fractures. Two distinct flow systems—local and regional—are identified based on pumping test analysis as well as hydrochemical and isotopic data. Drawdown curves

derived from pumping tests indicate that the behavior of the saturated layers, whose main porosity is given by the fracture network, corresponds to a confined aquifer. Pumping tests also reflect a double porosity within the system and the occurrence of impervious boundaries that support a compartmentalized model for the whole aquifer system. Hydrochemical data and associated spatial evolution show the result of water–rock interaction along the flow lines. Concentration of magnesium, derived from dolomite dissolution, is a tracer of the flow-path along distinct stratigraphic units. Water stable isotopes indicate that evaporation (near a 5% loss) occurs in a thick unsaturated zone within the massif before infiltration reaches the water table. The hydrogeological analysis of this outcropping system provides a methodology for the conceptualization of groundwater flow in similar buried systems where logging and hydrogeological information are scarce.

**Electronic supplementary material** The online version of this article (doi:10.1007/s10040-017-1618-9) contains supplementary material, which is available to authorized users.

✉ Marc Anglés  
marc.angles@outlook.es

<sup>1</sup> Escuela de Ingeniería de Procesos Industriales, Facultad de Ingeniería, Universidad Católica de Temuco, 4510721 Temuco, Chile

<sup>2</sup> Departament d'Enginyeria Civil i Ambiental, Universitat Politècnica de Catalunya-BarcelonaTech, 08034 Barcelona, Spain

<sup>3</sup> Unitat Associada: Grup d'Hidrologia Subterrània (UPC-CSIC), Barcelona, Spain

<sup>4</sup> Unitat d'Estratigrafia, Departament de Geologia, Facultat de Ciències, Universitat Autònoma de Barcelona, 08193 Bellaterra, Spain

<sup>5</sup> Grup de Geologia Aplicada i Ambiental (GAiA), Centre de Recerca en Geologia i Cartografia Ambiental (Geocamb), Dep. de Ciències Ambientals, Universitat de Girona, and Catalan Institute for Water Research (ICRA), 17003 Girona, Spain

**Keywords** Lithostratigraphy · Hard-rock aquifer · Hydrochemistry · Stable isotopes · Spain

## Introduction

Groundwater is an important resource in many areas of the world because of its widespread distribution compared to that of surface water. Many areas rely on consolidated sedimentary rock aquifers whose hydrogeological properties are related to secondary processes such as fracturing or dissolution. Their geological architecture is hence highly heterogeneous and, therefore, it controls groundwater flow magnitude and direction along preferential flow paths.

Studies of alluvial fan aquifers are usually based on limited geological data that simply provide a general description of these systems. Such studies include the Choshui fan-delta in Taiwan (Chen and Liu 2003, 2005; Peng et al. 2014), and the

Dead-Sea fan deltas in the Middle East (Yechieli et al. 2010). These studies are based on subsurface data that describe the rock bodies' geometry, permeability, barrier locations, and other hydrogeological features. The lithostratigraphy and basement/boundary features of these formations can greatly affect groundwater flow and its quality. In this sense, lithological variations may lead to variation in concentrations of natural substances (i.e., hardness, sulfate, sodium and/or trace elements) that affect the quality of groundwater resources (Li et al. 2014; Mas-Pla et al. 2016).

From a sedimentological point of view, alluvial fans and alluvial fan deltas have been extensively studied (Arenas et al. 2001; Benvenuti 2003; Blair 2000; DeCelles et al. 1991; Harvey et al. 2005; Sohn et al. 1999), as well as their relationship with fossil fuel and groundwater resources (e.g., Galloway and Hobday 1996). Petroleum geology methods such as facies modeling and geostatistics have also been applied to deltaic and alluvial systems such as the one studied and reported in this paper; hence, stratigraphic and sedimentological features are well known for these geological system (e.g., Cabello et al. 2011).

In order to contribute to the understanding of the hydrogeological processes in fossil fan deltas in mountain areas, this paper presents a stratigraphic and hydrogeological study of the Paleogene fan delta of Sant Llorenç del Munt (Barcelona, NE Spain), a well-exposed mountain range massif with extensive and clear outcrops, with numerous springs and some groundwater exploitation wells. Such particularities allow characterization of its hydrogeological system in detail, as an example of these groundwater flow systems. This paper describes a hydrogeological conceptual model by integrating geology (tectonic structure, stratigraphy, lateral sedimentary changes, mapping and subsurface data) and groundwater hydrology (pumping tests, major ion hydrochemistry and environmental isotopes). The focus is especially on how the overall flow pattern and water resources storage are affected by the less permeable rock types and the structural setting of the massif.

## Study area

The study area is located in the SE margin of the geological Ebro Basin, and it is attached to the Catalan Coastal Ranges (Fig. 1a,b). The Cenozoic Ebro basin is a foreland basin bounded by three mountain ranges: the Pyrenees to the North, and the Catalan Coastal Ranges (CCR) and the Iberian Ranges to SE and SW, respectively. During the middle and late Eocene this basin was connected to the Atlantic Ocean and at the basin margin several fan deltas developed, including that of Sant Llorenç del Munt (Maestro 1987; López-Blanco 1996). Sediment source areas from SE fans were the CCR, which constituted an Alpine fold and thrust

belt containing a Variscan basement and a Mesozoic cover (Anadón et al. 1985a, b; López-Blanco 1994, 2006).

The subaerial part of this delta corresponded to an alluvial fan with a proximal area dominated by gravel-size sediments, and in the distal part, sand and mud accumulated. In its submarine part, a sandy delta front and a muddy prodelta also developed. Episodes of carbonate sedimentary deposition on the shelf are also found in the stratigraphic series. Presently, all these sediments are found as cemented rocks, and they constitute an isolated mountain massif (mainly conglomerate and sandstone) of 1,104-m maximum altitude above sea level (asl), with nearly 600-m reliefs. The massif undergoes differential erosion depending on the different resistances to denudation of its distinct sedimentary layers and tectonic elements (faults and joints).

Two distinct typologies of fractures have been described in the Sant Llorenç del Munt conglomeratic formations: interjoints and megajoints (Andrés 1964; Freixes 1986). Interjoints are preferentially developed in meter-thick layers that show a fragile behavior under tectonic stress. Megajoints cross the whole conglomerate bodies with thicknesses from tens to hundreds of meters. Lithology, grain size and thickness of each lithofacies type (i.e., the sedimentary facies) define the fracture pattern, and consequently the hydraulic connectivity within each unit, as stated by Alsaker et al. (1996) for the nearby and geologically equivalent Montserrat massif conglomerates. In broad terms, fracture frequency is higher as bedding thickness and grain size decreases, creating a heterogeneous spatial (horizontal as well as vertical) distribution of porosity which is paramount to describe the hydrogeological behavior and water resources yield of alluvial fan sedimentary formations.

Average climatic conditions in the area, according to the three observatories located at altitudes between 321 and 528 m asl, are mean temperature of 13.30 °C, precipitation of 624 mm, and actual evapotranspiration of 488 mm, which represents 78.3% of the mean precipitation. The population of the municipalities included in the study area is 58,885 inhabitants (IDESCAT 2016). Water supply relies on water transfer from other basins (Llobregat-Ter), so groundwater resources basically satisfy 30% of the population needs. No significant agricultural demand exists in the area. Land use in the study area is mainly Mediterranean forestry (89.4%) rather than agriculture (1.2% in 2000; Grau et al. 2007).

## Methods

### Geological methods

Information on surface geology was acquired by geological mapping and rock characterization. Geological mapping for the central Sant Llorenç del Munt fan delta was mainly

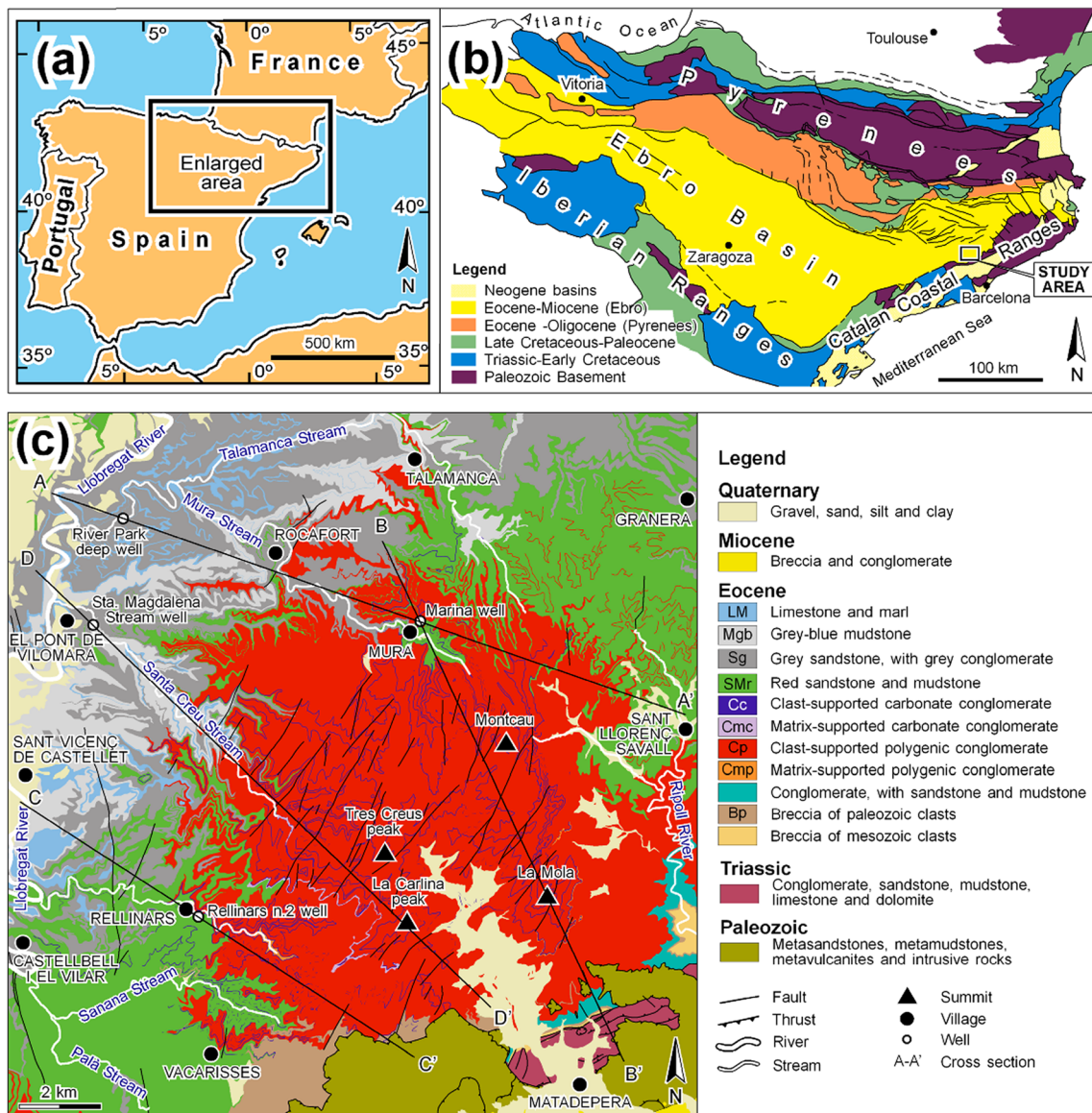


**Fig. 1** a–b Geographical and geological setting of the Ebro Basin; c Geological map of the study area

conducted at 1:5,000 scale (Anglés and Maestro 2010–2011), while for the surrounding areas, the 1:25,000 geological map was redrawn (after ICGC 2003, 2010, 2011a, b). The geological map is summarized in Fig. 1c and it constitutes the basis for drawing distinct cross sections of hydrogeological interest that also include borehole information. Geological mapping and depositional system analysis have enabled identification of the main lithological units. More importantly, they have determined the spatial distribution and geometry of the main lithological units, accounting also for structural elements such as fractures, to build up a basic hydrogeological framework of the system. Field measurements of fracture densities in the sedimentary formations also complement the hydrogeological information.

Field observation records provided rock descriptions and parameters such as lithology, conglomerate grain

composition, color, texture (grain size, sorting), porosity, internal structure and morphology of rock bodies (morphology and lateral fingering of different rock types) and the occurrence of faults and joints. Representative samples from all rock types were used to obtain 16 thin sections. Two staining methods were used: yellow dye to visualize porosity, and Alizarin Red S and potassium fericyanide for the determination of calcite (Lindholm and Finkelman 1972). Two types of porosity were observed in the petrographic microscope: microfractures and, in lesser proportion, intergranular porosity. Percentages of porosity vs particles and cement were evaluated with comparison charts. Based on optical mineralogy, the main constituents of the sandy fraction and cement were identified. This provided percentages of silicate minerals, calcite, dolomite and others (see details in Anglés 2013). This

characterization is of paramount importance to correlate rock units with hydrogeological and hydrochemical features.

## Hydrogeological methods

### Well testing

Three pumping tests were carried out in July 2012 at wells: S.LL-22 (300 m depth), S.LL-31 (335 m) and S.LL-27 (389 m). Data from two essays from the year 2008 (by Elèctrica Pintó SL) have been revisited for S.LL-24 (51 m) and S.LL-25 (164 m). Tests were conducted once recovery was completed from previous pumping periods. Tests consisted of pumping and recovery time spans lasting between 2 and 4 h. The hydraulic head during the test was measured manually with a water-level meter.

### Hydrochemical sampling and analysis

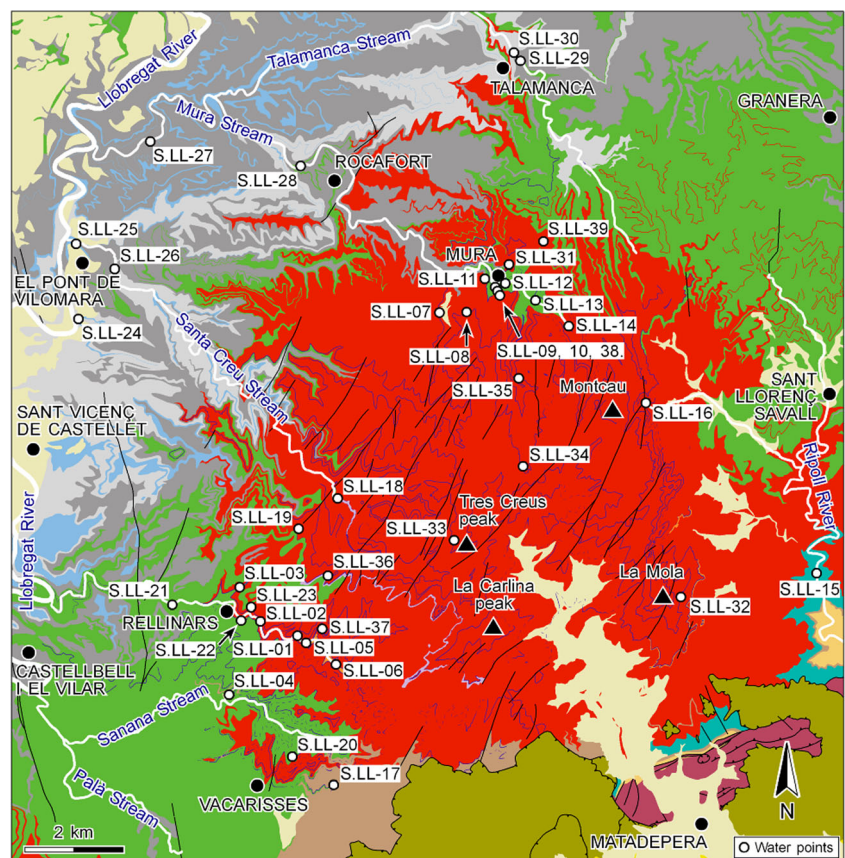
The hydrochemical dataset consists of 31 and 38 water samples collected during two field surveys—summer 2011 and spring 2012, respectively—coinciding with periods of drought and rain, respectively. Sampling points (Fig. 2)

account for 28 natural springs and 11 wells with depths between 4 and 389 m. Five sampling sites of the total are not directly located on the Eocene substrate (S.LL-04, S.LL-09, S.LL-10, S.LL-28 and S.LL-38), but they correspond to Quaternary sedimentary deposits, most of them alluvial formations, located along the Sant Llorenç del Munt drainage network. Water stable isotopic data—oxygen-18 ( $\delta^{18}\text{O}$ ) and deuterium ( $\delta\text{D}$ )—were only collected during the summer 2011 survey.

Samples for hydrochemical and isotopic analysis were taken from natural springs and active water supply wells. At least three casing volumes were removed from each bore prior to sampling, therefore samples are an integration of all productive layers along the borehole. Physicochemical parameters (pH, electrical conductivity, and temperature) were measured in situ using a flow cell to avoid contact with the atmosphere. After filtration (0.45  $\mu\text{m}$ ), samples were processed in the field and stored at 4 °C in a dark environment for subsequent transport and analyses.

In the laboratory, alkalinity (as  $\text{HCO}_3^-$ , since  $\text{pH} < 8.2$ ; mean  $\text{pH} = 7.39 \pm 0.04$  in 2011, and  $7.22 \pm 0.05$  in 2012) was measured by titration (METROHM 702SM Titrino). Anion ( $\text{NO}_3^-$ ,  $\text{SO}_4^{2-}$  and  $\text{Cl}^-$ ) content was measured by Capillary Electrophoresis (Agilent Technologies) using indirect UV detection;

**Fig. 2** Location of the water points studied at the Sant Llorenç del Munt fan delta (legend as in Fig. 1c)



concentrations of  $\text{Na}^+$ ,  $\text{K}^+$ ,  $\text{Ca}^{2+}$  were measured by Inductively Coupled Plasma-Optical Emission Spectrometry (ICP-OES, Perkin Elmer 4300 DV). The quality of the chemical analysis was checked by performing an ionic mass balance, with an error lower than 5%. Water stable isotopes were analyzed in a Finnigan Matt Delta S Isotope Ratio Mass Spectrometer (IRMS) coupled to an automated line based on the equilibration between H-water and  $\text{H}_2$  gas with a Pt catalyst, and between O-water and  $\text{CO}_2$  gas following standard methods (Epstein and Mayeda 1953). Notation is expressed in terms of  $\delta\text{‰}$  relative to the international standards V-SMOW (Vienna Standard Mean Oceanic Water) for  $\delta\text{D}$  and  $\delta^{18}\text{O}$ . The precision ( $\equiv 1\sigma$ ) of the samples, calculated from international and internal standards systematically interspersed in the analytical batches, were  $\pm 1.5\text{‰}$  for  $\delta\text{D}$  and  $\pm 0.2\text{‰}$  for  $\delta^{18}\text{O}$ .

## Results

### Geology

Ten distinct rock types (i.e., lithofacies) have been identified in the Sant Llorenç del Munt system (SLMS) on the basis of distinctive lithologic, mineralogical, textural and hydrogeological features which are described in detail in Table 1 and summarized in Figs. 3 and 4. Indeed, the main groundwater flow in the SLMS is basically dependent on fractures (joints and faults, see Andrés 1964; Freixes 1986; Alsaker et al. 1996), since intergranular porosity is very low (<5%).

The following 10 rock types, summarized in Table 1, are ordered from coarser to thinner grain size (i.e., from proximal to distal sedimentary facies):

- *Clast-supported polygenic conglomerate (Cp)*. This is the most widespread lithofacies of the SLMS massif (26% of its surface). The polygenic composition of its grains is due to the different origin of the source rocks, mainly belonging to the Variscan basement (e.g., Paleozoic phyllites and other crystalline rocks). Grains are clast supported, and matrix is sandy. The cement is calcitic. Thin-section determinations have established a microporosity value around 1–5% of the sample surface (i.e., microfractures plus intergranular porosity). This lithology creates homogeneous packages of massive conglomerate, facilitating the development of penetrative and spaced joints and faults that easily exceed 100 m of vertical extension.
- *Clast-supported carbonate conglomerate (Cc)*. This type accounts for only 7% of the SLMS surface, but is of particular hydrogeological importance. The clast-supported carbonate conglomerate is predominantly composed (around 80% of the grains) of carbonate Mesozoic cobbles (mainly derived from Triassic rocks). The matrix is sandy and it has low clay and silt content. The cement is calcitic. These deposits are widely spread throughout the alluvial fan system and each deposit has a maximum thickness of 20–30 m. They are interbedded with type Cp. Microporosity (i.e., microfractures plus intergranular porosity) is between 1 and 5% of the sample surface. Significantly, this type presents a closely spaced fracture network that represents the sum of interjoints (Andrés 1964), which are restricted to Cc beds, plus background joints (megajoints) and the faults that affect the conglomeratic formation as a whole (Fig. 5a).
- *Gray conglomerate (Cg)*. This has a gravel framework and a sandy matrix with few silts and clays. Its outcropping percentage across the system is around 7% in areal extent. They are deposited in front of the Cp and Cc types (Fig. 3). Laterally, these gray conglomerates are connected to the proximal conglomerates and evolve to sands towards the inner basin areas. They may have a dense fracture network. This is a relevant rock type for subsurface water dynamics, since it connects conglomerates with gray sandstone layers (Sg).
- *Matrix-supported polygenic conglomerate (Cmp)*. This type accounts for around 5% of the SLMS and is found as limited layers within Cp conglomerate layers. The fracturing pattern resembles that of type Cp. The fracture pattern is in continuity with Cp joints, except in the thicker Cmp layers.
- *Matrix-supported carbonate conglomerate (Cmc)*. This type accounts for around 5% of the SLMS, and is found as limited layers within Cc conglomerates. In both cases, the matrix of the Cmp and Cmc is constituted by sandy/muddy sediments of siliceous composition. Microporosity is around 1–5%, and fractures are poorly defined (except in the small layers interbedded within Cp or Cc).
- *Breccia of Paleozoic clasts (Bp)*. This type has a small surface extension of around 2% of the SLMS (Figs. 1c and 4), and, because of this, it is not actually relevant for this study. It has a muddy matrix-supported texture which is responsible for low granular porosity. Also, its internal disorganization contributes to create a poorly developed fracture network. No aquifers have been assigned to this rock type, and it is considered as an aquitard. Detailed description of these levels is found in Anadón (1978).
- *Red sandstone and mudstone (SMr)*. This is an interbedded type that has a very poor to moderate sorting. It accounts for around 22% of the SLMS, and it mainly appears in the distal alluvial fan and fan fringe areas (with maximum extent of 1.5 km in front of the alluvial fan). Microporosity is around 1% (mainly microfractures). Fractures are restricted to sandy layers, and they do not propagate into the bounding mudstones.

**Table 1** Main lithofacies of the Sant Llorenç del Munt with summarized features

Rock types	Lithology and color	Texture/selection	Granulometry <sup>a</sup>	Percentage of whole rock mineralogy <sup>b</sup>	Morphology of sedimentary bodies <sup>a</sup>	Internal structures	Genetic interpretation	Depositional environment	Fracturation (m/ joints)
Breccia of Paleozoic clasts (Bp)	Mudstone and sandstone breccia, dark red or brown	Matrix-supported to clast-supported	Clast: max 20–28 cm Matrix: mud-sand	SIL: 98.8, CAL: 1.2	Lenticular Thickness: dm-m Continuity: hm	Disorganized or fining upward	Debris flow	Colluvial	Poorly defined
Clast-supported polygenic conglomerate (Cp)	Dark red conglomerate	Clast-supported	Clast: max 160 cm Matrix: sand with little mud	SIL: 69.9, CAL: 5.8, DOL: 24.2, OTHERS: 0.1	Tabular or channelized Thickness: max 2.2 m Continuity: m-dam	Horizontal bedding and cross bedding	Aqueous flow: laminar, braided or with some sinuosity	Proximal and distal alluvial fan	8.1 35.0 37.3 87.5
Clast-supported carbonate conglomerate (Cc)	Gray conglomerate	Clast-supported	Clast: max 100 cm Matrix: sand	SIL: 19.2, CAL: 13.4, DOL: 67.3, OTHERS: 0.1	Tabular or channelized. Thickness: max 1.7 m. Continuity: m-dam	Horizontal bedding and cross bedding	Aqueous flow: laminar to braided	Proximal and distal alluvial fan	5.2 6.2 6.3 8.6
Matrix-supported polygenic conglomerate (Cmp)	Sandstone-mudstone conglomerate, red	Matrix-supported	Clast: max 200 cm Matrix: sand-mud	SIL: 73.7, CAL: 3.4, DOL: 22.2, OTHERS: 0.7	Tabular or lenticular Thickness: max 2.6 m Continuity: m-hm	Coarsening upward, fining upward or disorganized	Debris flow to hyperconcentrated flow	Proximal alluvial fan	Poorly defined
Matrix-supported carbonate conglomerate (Cmc)	Sandstone-mudstone conglomerate, red-orange	Matrix-supported	Clasts: max 380 cm Matrix: sand-mud	SIL: 42.6, CAL: 8.2, DOL: 47.9, OTHERS: 1.3	Tabular or lenticular Thickness: max 3.8 m Continuity: m-hm	Coarsening upward, fining upward or disorganized	Debris flow to hyperconcentrated flow	Proximal alluvial fan	Poorly defined
Red sandstone and mudstone (SMr)	Sandstone and mudstone, red	Very poorly sorted to moderately sorted	Sand-mud and mud	Sandstone: SIL: 90.9, CAL: 5.1, DOL: 1.0, OTHERS: 3.0	Tabular, lenticular or wavy sandstone, alternate with mudstone Thickness: cm-m Continuity: m-hm	Massive, fining upward, horizontal bedding and cross bedding	Aqueous flow: sheet flood and overflow channel	Distal alluvial fan	0.4 0.7 1.2
Gray conglomerate (Cg)	Gray conglomerate	Clast-supported or matrix-supported	Clast: cm order. Matrix: sand with little mud	SIL: 68.8, CAL: 8.8, DOL: 20.4, OTHERS: 2.0	Tabular to lenticular. Thickness: dm-m. Continuity: dam-hm	Cross bedding	Aqueous flow of distributary mouth bar	Delta front	2.2 2.5
Gray sandstone (Sg)	Gray sandstone	Moderately sorted to very well sorted	Sand	SIL: 55.6, CAL: 29.3, DOL: 5.1, OTHERS: 10.0	Tabular, lenticular or wavy. Thickness: cm-m. Continuity: dam-hm	Horizontal bedding and cross bedding	Aqueous flow of distributary mouth bar	Delta front	0.9 2.7
Gray-blue mudstone (Mgb)	Carbonated mudstone or marl, gray-blue	–	Silt and/or clay	Highly variable (carbonate and clays)	Tabular	Massive	Decantation	Prodelta	Poorly defined
Limestone and marl (LM)	Gray limestone and blue-gray marl	Packstone, grainstone or boundstone	–	Limestone: SIL: 13.1, CAL: 84.9, DOL: 0.0, OTHERS: 2.0	Tabular	Massive, nodular bedding or organic structure	Biochemical carbonate precipitation	Carbonate platform	2.4 4.8

<sup>a</sup> Magnitude order: centimetric (cm), decimetric (dm), metric (m), decametric (dam), hectometric (hm)<sup>b</sup> Mineralogical composition as percentage of: silicate minerals (SIL), calcite (CAL), dolomite (DOL), and opaque minerals and organic matter (OTHERS) (after Anglés 2013)

- *Gray sandstone (Sg)*. This type has a moderate- to well-sorted grain size. It accounts for around 15% of the SLMS, and these layers are arranged in thickening and coarsening upwards cycles that have a thickness of decameters order. These cycles (Fig. 3) have a succession that begins with marls (Mgb) and progress towards enriched sandstone layers (strictly, Sg) to finally evolve to gray conglomerates (Cg; Fig. 5b). These cycles provide well defined Sg and Cg units vertically isolated between marl layers (Mgb).
- *Gray-blue mudstone (Mgb)*. This type shows a marl composition, and it has a bulky appearance. It accounts for around 9% of the SLMS area. Despite its loose appearance due to weathering, with a badland morphology where it outcrops, the fresh rock is cohesive and it stands as a clear groundwater flow barrier because of its low hydraulic conductivity.
- *Limestone (LM)*. This alternates with marls and has a packstone to grainstone texture. The matrix is micritic and, locally, is a boundstone. Stratification is massive and nodular and it provides tabular rock bodies with

thickness of meters to decameters order. It accounts for around 2% of the SLMS, and laterally and basinward evolves to Sg and Mgb, respectively. Microporosity is around 1% and fractures are well developed.

As observed in Figs. 3 and 4, all these rock types present as lateral-facies changes that grade progressively from proximal alluvial conglomerates (Cp, Cc, Cmp and Cmc) to distal alluvial sandstones and mudstone (fan fringe, SMr), to delta front sandstones and conglomerates (Sg, Cg) and prodelta marls (Mgb). Shallow-water limestones (LM) grade laterally both to Mgb and Sg. The obtained correlation, based on geological data, defines the architecture of rock types Sg, Cg and Mgb (Fig. 4, cross section A–A') which is the result of the ancient sea level relative fluctuations. Successive regressions and transgressions forced the emplacement of the delta front as a result of relative sea level lowstands and highstands, respectively. As discussed later, the

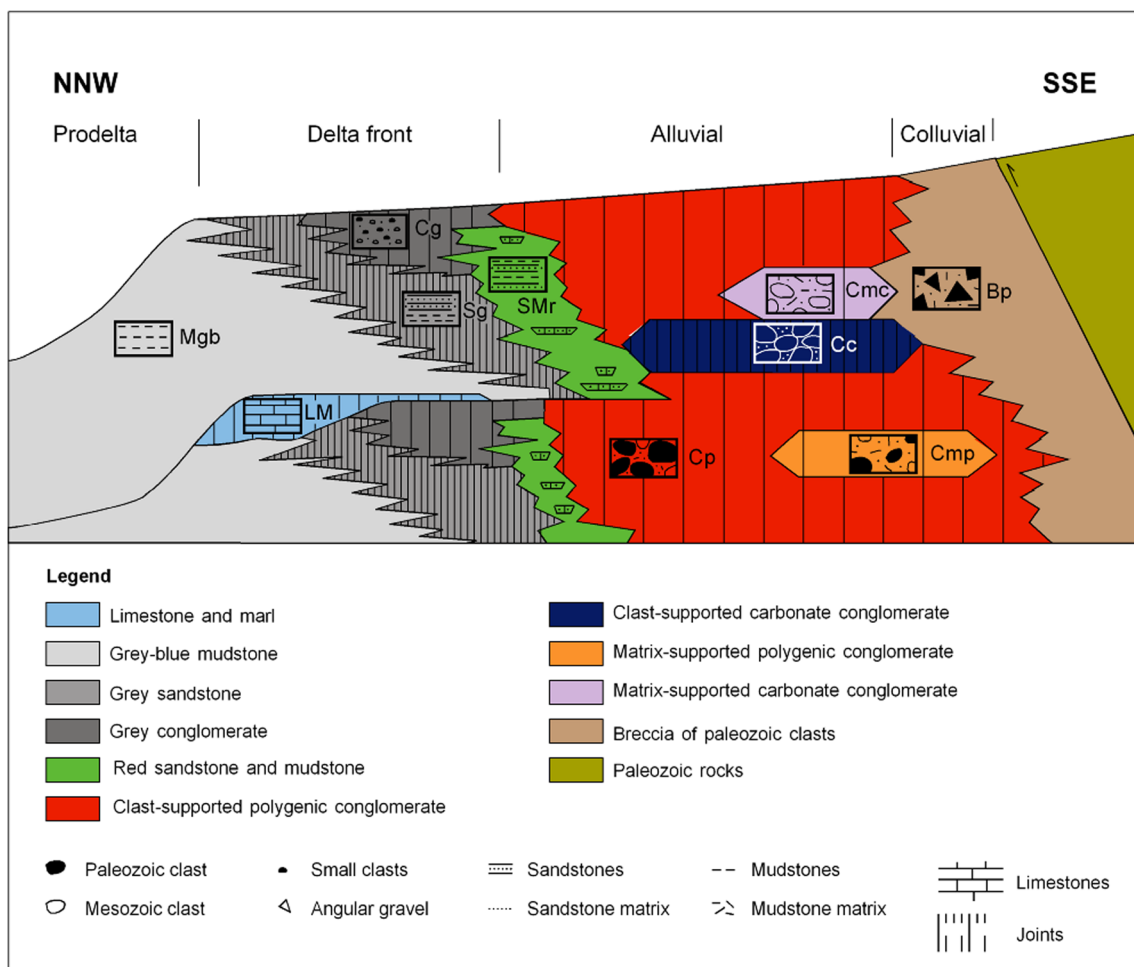
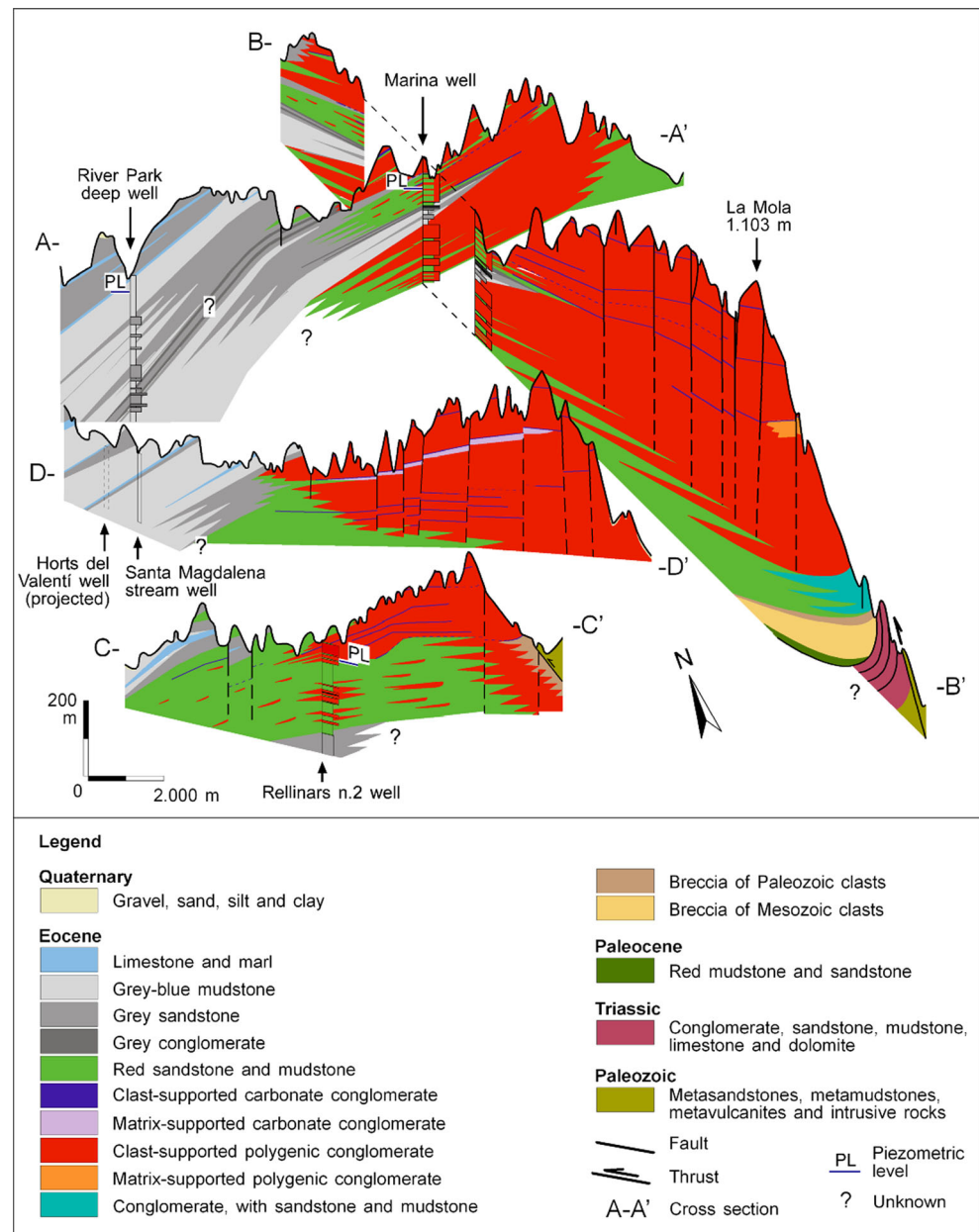


**Fig. 3** Depositional environments of the Sant Llorenç del Munt fan delta with the main lithological features of the rock types. Fracture density is represented by *differently spaced vertical lines*

**Fig. 4** Cross sections along the Sant Llorenç del Munt fan delta (see location in Fig. 1c)



basinward shift of Cg during maximum progradation episodes are particularly relevant for the hydrodynamics of the system.

## Hydrogeology

The lack of wells and observations points (boreholes) within the Sant Llorenç Range prevents both the setting of approximate hydraulic head values in the study area and the defining of an approximate potentiometric map for the massif. Indirect knowledge could be derived from the altitude of spring occurrence—Tables S1 and S2 of the electronic supplementary

material (ESM)—yet their location depends on diverse geological factors that impede reporting any reliable cartography.

Hydraulic head measurements were acquired, manually or with pressure loggers, at the same supply wells as where the pumping tests were conducted. Well stratigraphy, screened intervals and test details are given in Table 2, showing that some wells can be understood as exploiting a multilayered aquifer of similar lithological/stratigraphic characteristics in all their depths; thus, head values represent an averaged value of all layers. In this sense, maximum head elevations were recorded at 191, 325, and 455 m asl for wells S.LL-27, S.LL-22, and S.LL-31, respectively, corresponding to the integrated head among all productive layers crossed by the



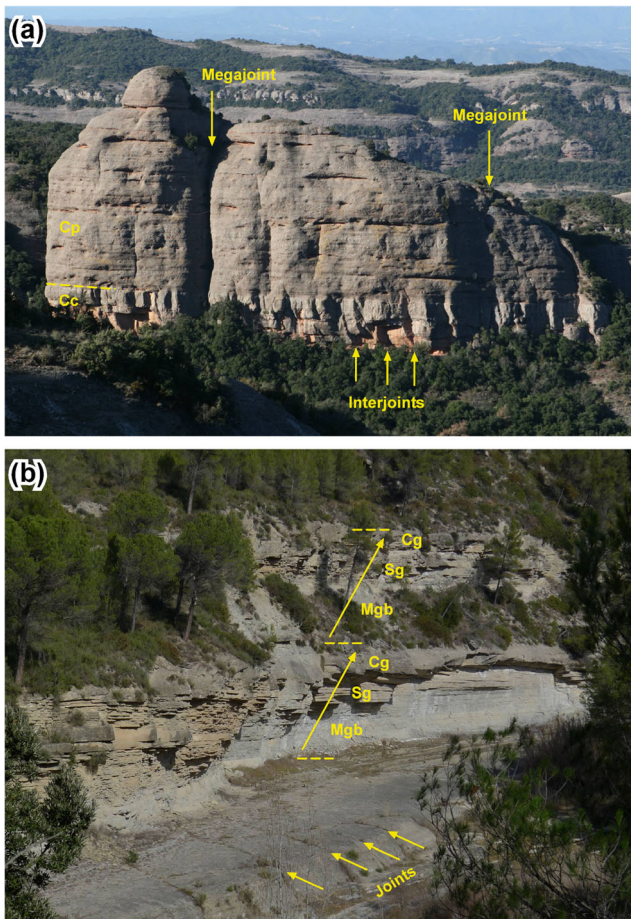


**Fig. 5** **a** The Falconera cliff displaying megajoints affecting both  $C_p$  and  $C_c$  layers, and interjoints affecting solely the  $C_c$  bed; **b** The Talamanca stream displaying the thickening and coarsening upwards front deltaic sequences which show the following order (from base to top):  $Mgb$ ,  $S_g$  and  $C_g$

borehole. Inside the Sant Llorenç del Munt range, stratigraphic layers and discontinuities produce perched aquifers that are the origin of the multiple springs disseminated along the Sant Llorenç del Munt massif.

Continuous head records in wells S.LL-31 and S.LL-27 showed some immediate response to rainfall events with a time lag of a few days (range 1–6 days; Anglés 2013, Figs. S1 and S2 of the *ESM*). This suggests that pressure variations from the recharge areas are efficiently registered in these wells. Despite the multilayered nature of these boreholes and their daily pumping activity, some interpretations can be made. Thus, the time lag between the rainfall event and the pressure increase is interpreted as the time needed for recharging water to cross the unsaturated zone and reach the water table, whereby the increase of head will be recorded as a pressure increase in the well records. This is consistent with the hydrochemical and isotopic data.

A diagnostic analysis of the pumping tests performed at constant discharge has been conducted based on the

logarithmic derivative of the drawdown ( $\partial s/\partial \ln t$ ) as a function of time in the log-log scale (Renard et al. 2009). The logarithmic derivative is sensitive to variations of the shape of the drawdown curve, so this method detects behaviors that would otherwise remain unnoticed. Derivative plots reveal a diminution of the derivative value which is attributed to the effect of a potential double porosity of geological relevance as the derivative value recovers after its former decrease (Fig. 6). Double porosity responses are noticed in wells S.LL-22 and S.LL-31. In particular, well S.LL-22 shows this behavior at early time (5 min), followed by progressive increase of the derivative value. Conversely, well S.LL-31 shows a complex behavior between 15 and 50 min, approximately, that later recovers to a smooth curve. The double porosity effect is associated with the later smooth decrease (40–50 min), while the first unordered decrease (15–20 min) is attributed to the effect of small, local heterogeneities of the media. The pumping test at well S.LL-27 also shows a decline in its derivative value after 30 min, attributable to a double porosity effect, yet its drawdown and derivative value abruptly increase as a result of the effect of a no-flow boundary.

The Theis equation was used to simulate drawdown at a distance similar to well radiuses, being aware that this assumption represents an approximation to the actual drawdown, reporting the fitted values of transmissivity ( $T$ ) and storativity ( $S$ ) using the minimum square difference criteria between observed and simulated data (Fig. 6). Early-time linear behavior at well S.LL-27, with an approximate slope of 0.5, is associated with a major fault intersected by the well that only influences the early behavior, as after minute 10, the aquifer shows a radial flow according to the Theis model. Early-time discrepancies at well S.LL-31 are due to a well-storage effect. In each case, the Theis equation can thus be used to adequately estimate the hydraulic properties of the aquifer in the vicinity of the well restricted by the short duration of the tests. Nevertheless, it is significant, geologically speaking, that the double porosity effect and the occurrence of a no-flow boundary (S.LL-27) have been identified through the diagnostic analysis.

In addition, four pumping tests with variable pumping rate (Table 2, all except S.LL-27; Fig. 7) were also calibrated using an optimization algorithm that solves the Theis equation for variable linear discharge rates based on the formulation by Tsang et al. (1977), which uses Duhamel's superposition integral (Mas-Pla et al. 1999). This procedure allows a simultaneous simulation of drawdown, some with variable pumping rates, and recovery data at the borehole radius distances; this procedure was used because no observation wells were available near these production wells. According to this procedure, storage coefficient values can also be considered for the recovery analysis.

Tests at wells S.LL-22 and S.LL-31 had shorter duration (they lasted 120 and 240 min, respectively), and they were

**Table 2** Synthesis of the aquifer levels and hydraulic parameters of wells. *Aquifer levels* refers to the screened intervals in each well

Well	Depth (m)	Lithostratigraphic units (m deep)	Aquifer levels (m depth)	Piezometric level (m deep)	Pumping discharge (m <sup>3</sup> /d)	Pumping time/ recuperation time (d)	Transmissivity (m <sup>2</sup> /d)	Storage coefficient	
S.LL-22 Rellinars No. 2	300	0–30	Cp	45–54	29.60	240	0.08 / 0.08	14.40–15.60	0.31–0.36
		30–33	SMr						
		33–42	Cp						
		42–45	SMr						
		45–54	Cp						
		54–245	SMr + Cp						
S.LL-31 Marina	335	245–300	Sg	309–320	98.28	240	0.17 / 0.16	3.30–4.61	0.08–0.26
		0–51	Cp + SMr						
		51–54	Sg						
		54–130	Cp + SMr						
S.LL-24 Marquet Paradis	51	130–181	Cg + Sg + Mgb	12–13 33–36 42–48	9.58	Variable	1.00 / 0.10	4.40	0.12
		181–335	Cp + SMr						
		0–8	Quaternary deposits						
		8–33	Mgb						
S.LL-25 Horts Valentí	164	33–45	Sg	–	11.13	Variable	1.00 / 0.06	0.62	0.26
		45–51	Mgb						
S.LL-27 River Park	389	Sg and Mgb		109–130 157–163 190–196 239–272 275–281 312–348 354–363	43.70	240	0.09 / 0.17	0.61–0.70	0.28–0.35
		0–109	Mgb						
		109–130	Sg						
		130–157	Mgb						
		157–163	Sg						
		163–190	Mgb						
		190–196	Sg						
		196–239	Mgb						
		239–272	Sg						
		272–275	Mgb						
		275–281	Sg						
		281–312	Mgb + Sg						
		312–348	Sg + Cg						
348–351	Mgb								
351–363	Sg								
363–389	Mgb								

conducted under uniform withdrawal rate till the pumping ceased. Recovery was observed at each well. Hydraulic head simulations using fitted  $T$  and  $S$  values are able to concurrently reproduce the drawdown and the recovery limbs considering Theis assumptions, yet they fail to reproduce the maximum observed drawdown which seemed not to have attained a uniform depth by the time the pump was turned off (Fig. 7; Table 2). Based on the former analysis of drawdown derivatives, such difference between observed and simulated maximum drawdown for the best optimized  $T$  and  $S$  values at larger times is attributed to double porosity effects. In the SLMS

case, it is due to a change of fracture aperture, density or connectivity (as it can be seen in Fig. 5). Fitted values using the whole drawdown and recovery records (Fig. 7) brings out  $T$  and  $S$  values consistent with those using the Theis equation on the drawdown data only (Fig. 6), indicating that, on the whole, the exploited levels behave as for confined aquifers.

Pumping tests conducted at variable pumping rates in wells S.LL-24 and S.LL-25 had longer durations (24 h each), reaching a stabilized drawdown by the end of the pumping period (Fig. 6; Table 2). In the S.LL-24 test, the deep drawdown attained at 200 min, and which seems to persist until the

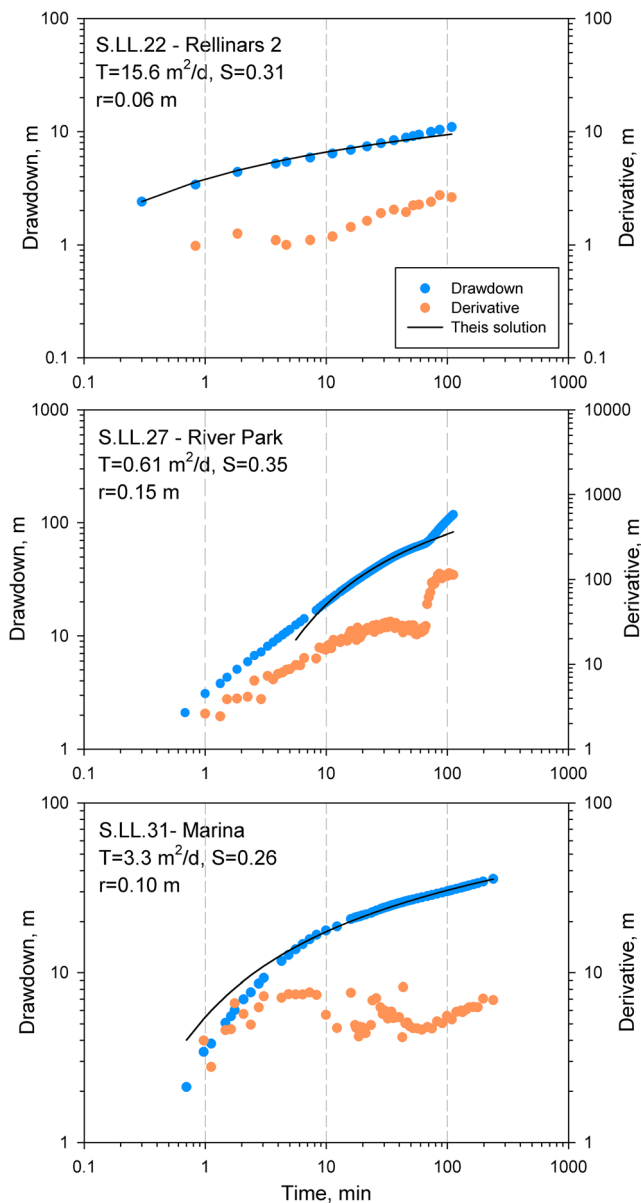


**Fig. 6** Diagnostic analysis using log-log plots of the three pumping tests conducted at constant discharge rate. Drawdown data are plotted jointly with their derivatives, along with fitted Theis solution

end of the pumping period, is not reproduced by the simulation even though well discharge variations are considered by the algorithm. This fact points out the influence of geological heterogeneity on the hydraulic response of the aquifer system, suggesting the role of discrete elements such as fractures. In the S.LL-25 well, however, the initial high drawdown caused by a pumping rate peak is well reproduced by the model, as well as the overall trend of the drawdown. This indicates that a more homogeneous rock volume is affected by this well depression cone. Its final drawdown was well reproduced in both tests, so the  $T$  and  $S$  values can be assumed to be representative of these hydrogeological units. Simulated recovery is slower than observed data in both wells.

The pumping test in well S.LL-27 brings out a clear example of the system's heterogeneity, as already discussed in the diagnostic analysis. Drawdown shows two distinct developed curves under a steady pumping rate (Fig. 8). The increased drawdown rate observed after 70 min points to the occurrence of some impervious boundary that significantly controls the flow towards the well, thus defining an aquifer of limited extent. Therefore, it would be inappropriate to use the Theis approach to solve for the hydrogeological parameters using the entire drawdown record; however, on the other hand, it is worth noting that both withdrawal segments also achieve clear straight lines in the semi-log plot (Fig. 8b), which permits the interpretation of the first reach using the Cooper-Jacob method. The transmissivity value ( $T = 0.70 \text{ m}^2/\text{d}$ ) is in the lower rank of those found in the other tests. The second segment indicates the existence of an impervious boundary, and it suggests that this multilayer aquifer (Table 2) can be considered, on the whole, a true confined aquifer because the drawdown data lie on a clear straight line. Furthermore, the  $S$  value is approximate and must be taken with caution, as the  $S$  value estimated by the Cooper-Jacob method depends on the distance from the observation well to the withdrawal well, and it has been taken in this analysis as being equal to the borehole radius. Unfortunately, the pumping test did not last long enough to observe whether a steady drawdown was finally reached; moreover, the lack of a true observation well does not allow for an estimation of the distance to the impervious boundary using the time at which the break of the slope takes place (e.g., Chapuis 1994).

The highest transmissivity values are found in well S.LL-22 ( $T = \text{approximately } 15 \text{ m}^2/\text{d}$ ) which is drilled in conglomerates (Cp rock type; Table 2). All other wells show lower values, the lowest found in the sandstone layers (Sg) interbedded within mudstone layers (Mgb) constituting a multilayered aquifer, as in well S.LL-27 ( $T = \text{approximately } 0.66 \text{ m}^2/\text{d}$ ). Consolidated strata as conglomerates and sandstones show dense fracture networks, and since their intergranular porosity is low ( $<0.05$ ) but the fitted storage coefficient values are quite large (approximately 0.25–0.30), it can be deduced that hydraulic conductivity mainly results from fractures and their interconnectivity. Nevertheless, differences between the observed drawdown data and reproduced drawdown curves based on Theis assumptions reveal the heterogeneity of the system as: (1) the occurrence of impervious boundaries attributed to lateral facies variations, as clearly observed in the S.LL-27 well; and (2) the occurrence of double porosity effects identified in the diagnostic analysis of these tests conducted at a constant discharge rate. Despite the importance of the fracture network in the recharge dynamics, these pumping tests also point out that the exploited 'aquifer levels' (i.e. the screened intervals in each well) mostly

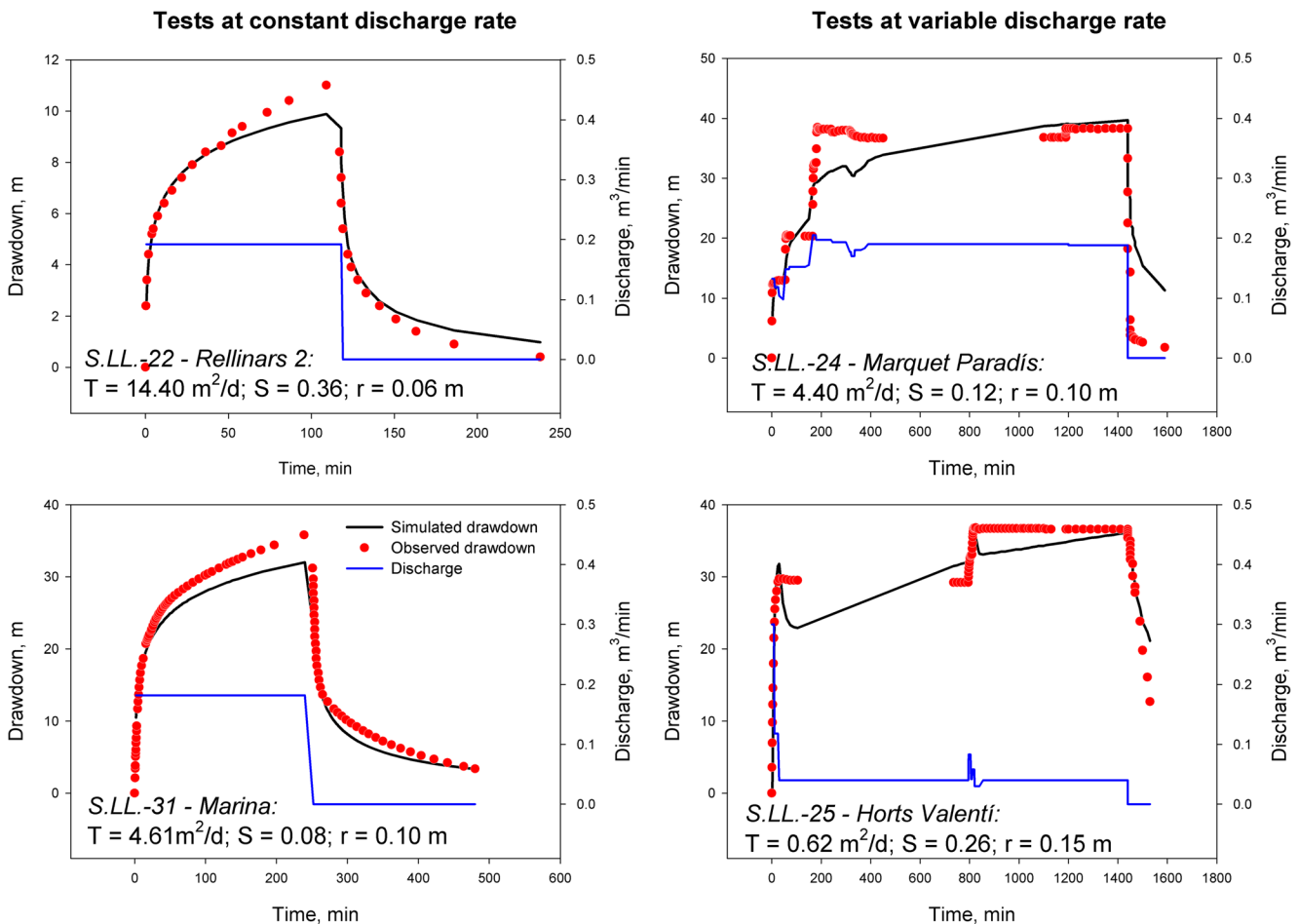


**Fig. 7** Pumping tests at wells S.LL-22, S.LL-24, S.LL-31, and S.LL-25 using a variable discharge approach (to include pumping rate variations as well as the recovery part) to fit transmissivity ( $T$ ) and storativity ( $S$ ) values according to the Theis solution (see text)

behave as confined aquifers, underlining the role of low-permeability layers (SMr and Mgb types) as confining units.

### Hydrochemistry

Based on the hydrochemical datasets of the field surveys carried out in the summer of 2011 and the spring of 2012 (Tables S1 and S2 of the [ESM](#)), several groundwater hydrochemical facies are defined according to their major components content and the drilled lithostratigraphic unit, as summarized in Table 3. No major hydrochemical changes are observed in the Piper plot between both surveys (Fig. 9), suggesting some steadiness in the system dynamics. Five hydrochemical groups are defined (A–E):

**Hydrochemical group A** This group is mainly defined by natural spring samples with a  $\text{HCO}_3\text{-Ca}$  facies that are hosted in Cp and SMr rock types. This is the dominant group, constituting 80% of the samples. Two other common characteristics of group A are its relatively moderate temperature (mean

$14.7 \pm 0.2 \text{ }^\circ\text{C}$  in 2011, and  $13.7 \pm 0.4 \text{ }^\circ\text{C}$  in 201; SM) and electrical conductivity (mean EC:  $702 \pm 16 \text{ } \mu\text{S}/\text{cm}$  in 2011, and  $694 \pm 16 \text{ } \mu\text{S}/\text{cm}$  in 2012, SM). Despite the high percentage of dolomite in Cp layers and Cc (24.2 and 67.3%, respectively; Table 1) groundwater samples in group A have a low Mg content, attributed to the low solubility of dolomite with respect to calcite. The low mineralization levels and the absence of dissolved Mg point towards a short transit time within these aquifer levels. Also within this group, natural springs S.LL-04, S.LL-06, S.LL-15, and S.LL-17 show slightly higher values of Na and Cl (increments of a few units of mg/L) that are attributed to weak cation exchange, as they do not stand out in the plots of Fig. 10. These ions cannot be associated with agricultural practices or human sources, as nitrate content is rather low (mean  $3.16 \pm 0.52 \text{ mg NO}_3/\text{L}$ ; Tables S1 and S2 of the [ESM](#); Menció et al. 2016).

**Hydrochemical group B** This group is represented by a single sampling point, the Marina well (S.LL-31), showing a water type  $\text{HCO}_3\text{-Ca-Mg-Na}$ . These well data, when compared with group A, stand out by its lower Ca content, yet

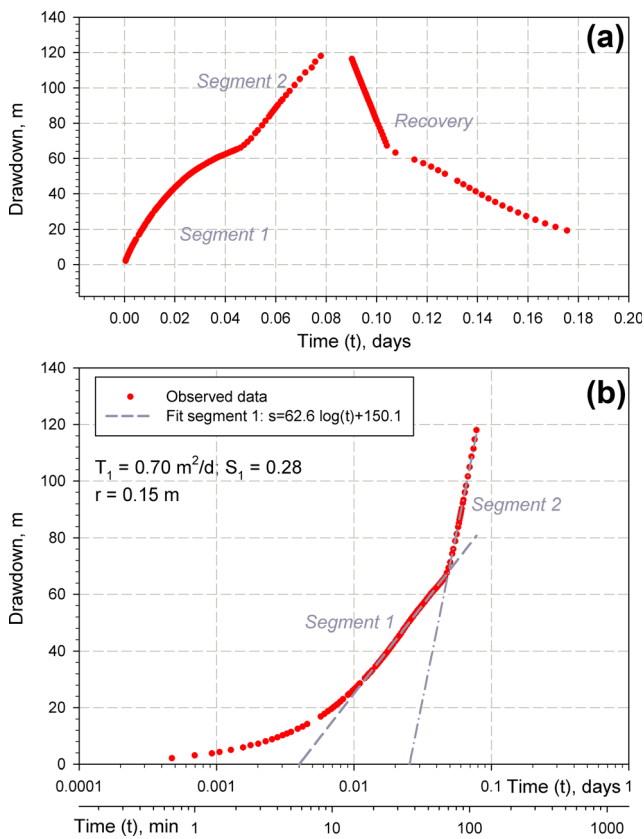


**Fig. 8** a Drawdown and recovery data at well S.LL-27 (River Park), and b pumping test analysis using the Cooper-Jacob method

have higher Na and Mg (Fig. 9). This fact could result from Na/Ca exchange related to clay occurrence in the SMr strata, which is found interlayered within Cp units (Fig. 4; Table 2), giving a high Na/Ca ratio (Fig. 10). However, the increase in Mg cannot be correlated to the hosting lithology as its percentage of dolomite is low (1.0% in SMr; Table 1); therefore, it must be assumed that the slow-flowing groundwater originating in the saturated zone of the Cp unit provides such Mg enrichment by dolomite dissolution. This hydrochemical composition, involving dolomite dissolution and cation

exchange processes, derives then from a larger water–rock interaction and a longer transit time of this sample compared to those of group A, which is consistent with the hydraulic properties of a sandstone and mudstone formation (SMr; Fig. 11).

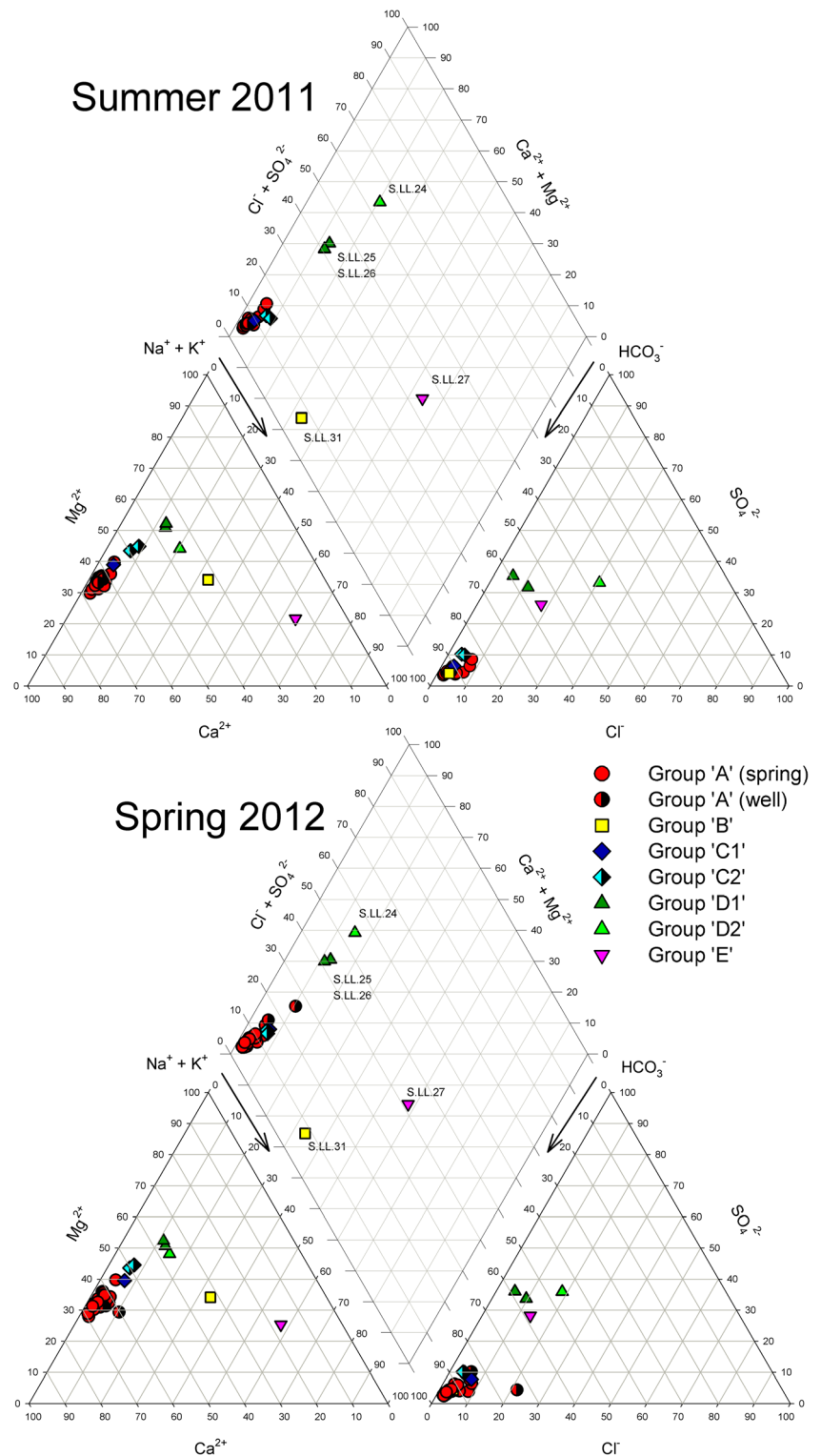
**Hydrochemical group C** Samples from this group are generally characterized by  $\text{HCO}_3\text{-Ca-Mg}$  facies which is attributed to the mineralogy of the gray sandstone (Sg) where wells are drilled (Fig. 9). Despite the general Mg enrichment shown by the group C samples, the different Mg content in samples from wells S.LL-29 and S.LL-30 justifies gathering them into a new subgroup (C2). Given the low proportion of dolomite in the gray sandstones (Table 1), it is assumed that Mg content is obtained in the preceding up-gradient formations such as Cp or Cc, and its subsequent flow across the delta front facies. Indeed, Sg rock types display surface efflorescences such as hexahidrite ( $\text{MgSO}_4 \cdot 6\text{H}_2\text{O}$ ) and epsomite ( $\text{MgSO}_4 \cdot 7\text{H}_2\text{O}$ ; Mata-Perelló 1990). Such occurrences of  $\text{SO}_4$ , attributed to pyrite oxidation, may enhance dedolomitization of the small dolomite content of the Sg sedimentary rocks, thereby adding some additional Mg to groundwater. Indeed, Otero et al. (2007) studied the Calderes and Mura streams (located 4 and 8 km to the northeast) which drain through similar lithologies and concluded that  $\text{SO}_4$  originates from the oxidation of pyrite which is found scattered (mineral dissemination) within the marl layers. Thus, dolomite (or Mg-rich calcite) and pyrite hosted in marine rock types can be dissolved by groundwater, enhanced by the occurrence of  $\text{SO}_4$ , and provide such high concentrations of Mg and  $\text{SO}_4$ .

**Hydrochemical group D** Samples from this group actually display a similar significant increase in the amounts of  $\text{SO}_4$  and Mg with respect to the former groups (Fig. 9), accompanied by an increase of EC ( $1,251 \pm 265 \mu\text{S}/\text{cm}$  in 2011, and  $1,135 \pm 198 \mu\text{S}/\text{cm}$  in 2012;  $n = 3$ ). This enrichment is due to potential groundwater pathways within the aforementioned rocks enhanced by dedolomitization processes within the

**Table 3** Main features of hydrochemical groups

Hydrochemical groups	Sampling points	No. of samples	Hydrochemical facies	Main productive lithofacies	Depositional environment
A	All springs, Rellinars Nos. 2 and 3 wells, Comes well	31	$\text{HCO}_3\text{-Ca}$	Cp + SMr	Alluvial fan
B	Marina well	1	$\text{HCO}_3\text{-Ca-Mg-Na}$		
C	C1 Rocafort well	1	$\text{HCO}_3\text{-Ca}$ ( $\uparrow\text{Mg}$ )	Sg	Delta front
	C2 Wells Recàrrega, Dipòsit	2	$\text{HCO}_3\text{-Ca-Mg}$		
D	D1 Wells Sta. Magdalena stream, Horts Valentí	2	$\text{HCO}_3\text{-Mg}$		
	D2 Marquet Paradís well	1	$\text{HCO}_3\text{-SO}_4\text{-Mg-Ca}$		
E	River Park deep well	1	$\text{HCO}_3\text{-Na}$		

**Fig. 9** Piper diagrams from the summer 2011 and spring 2012 surveys



sedimentary units of marine origin, rich in  $\text{SO}_4$  and Mg. Two distinct subgroups can be envisaged within group D:  $\text{HCO}_3$ -Mg-Ca (subgroup D1), and  $\text{HCO}_3$ - $\text{SO}_4$ -Mg-Ca (subgroup D2; Table 3). D1 samples (i.e., wells S.LL-26 and S.LL-25) are located downgradient from the main recharge area (i.e., the summit of the Sant Llorenç del Munt massif) following the

northwest dipping of strata, and they display an increase of the overall solute content ( $\text{EC} = 1,050 \mu\text{S}/\text{cm}$ ). The D2 subgroup is represented by the S.LL-24 well that is located in the Llobregat River Valley. The well profile and design, together with its geological setting (Table 2), discount any chance of surface-water recharge due to hydraulic connectivity with the

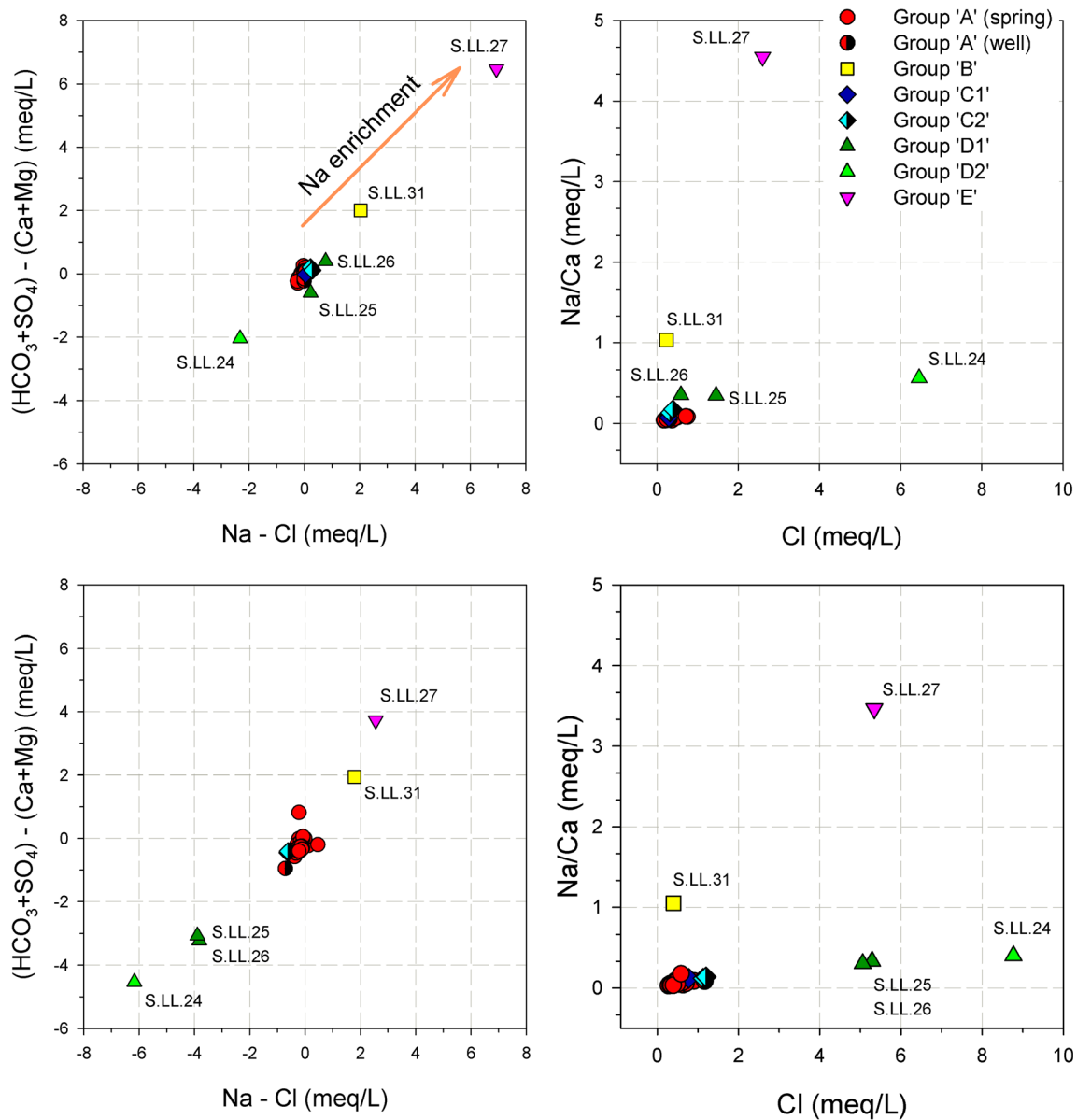


**Fig. 10** Binary plots related to the cation exchange Na/Ca, expressed as a difference of the main major constituents, and of the ratio Na/Ca vs Cl for the 2011 and 2012 surveys (*top* and *bottom*, respectively)

Llobregat River. Thus, its higher mineralization (1,768  $\mu\text{S}/\text{cm}$  in 2011) with respect to D1 (888 and 1,097  $\mu\text{S}/\text{cm}$ ) must be the result of intense subsurface water–rock interaction with a distinct pathway across the different lithological layers. Large values of  $\text{SO}_4$  and Cl, and the location of these wells in the hydrogeochemical conceptual scheme (Fig. 13), suggest a longer transit time.

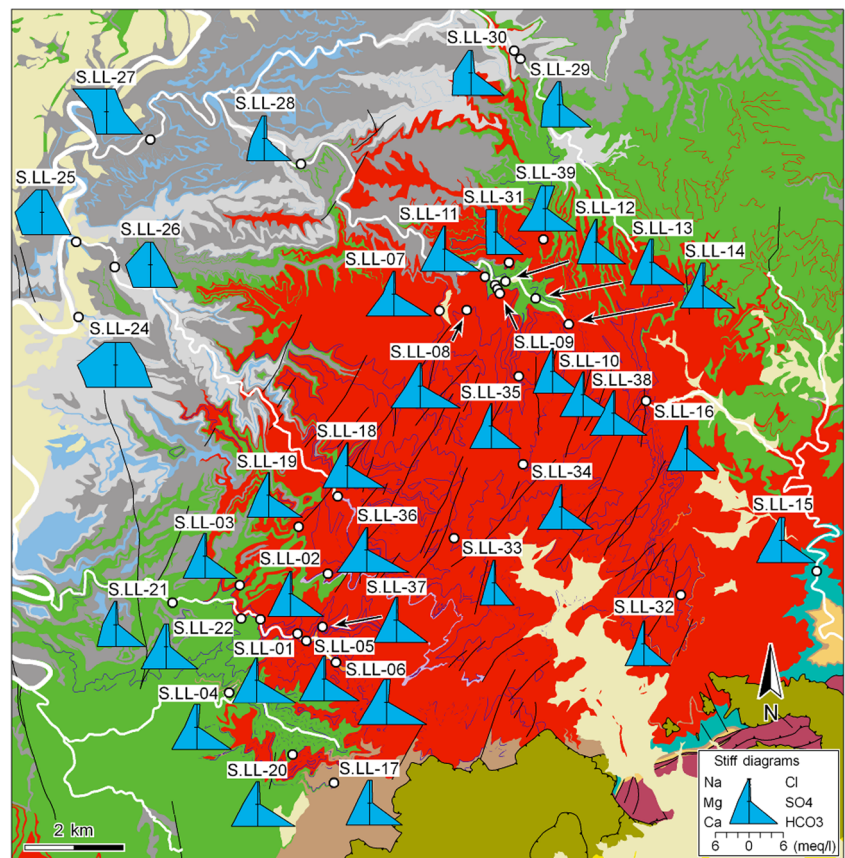
**Hydrochemical group E** This group is only defined at the S.L.L-27 deep well (389 m). It shows high EC values (1,291  $\mu\text{S}/\text{cm}$  in 2011, and 1,217  $\mu\text{S}/\text{cm}$  in 2012;  $n = 1$ ) and  $\text{HCO}_3$ -Na facies. These samples also present a high Cl content attributed to clay weathering; Ca depletion is interpreted as a

result of the cationic Na/Ca exchange that takes place in clay layers (Mgb layers; Fig. 10). The high chloride content and intense cationic exchange also implies long residence times (Tóth 1995, 2000; Carrillo-Rivera et al. 2007; Folch et al. 2011; Anders et al. 2014). This E group also shows some  $\text{SO}_4$  enrichment with respect to group A, reflecting the influence of marine rock types in the groundwater hydrochemistry.

#### Environmental isotopes ( $\delta^{18}\text{O}$ , $\delta\text{D}$ )

Groundwater stable isotope data (especially those of hydrochemical groups A and B) cluster together around mean values of  $\delta^{18}\text{O} = -8.17 \pm 0.04\text{‰}$  and  $\delta\text{D} = -49.05 \pm 0.20\text{‰}$ ,

**Fig. 11** Stiff diagrams from the spring 2012 field campaign (geological legend as in Fig. 1c)



in an area located above the Global Meteoric Water Line ( $\delta D = 8 \delta^{18}O + 10$ ; Craig 1961) in Fig. 12. The closest local meteoric line was defined at the Montseny Range, about 40 km NE and at an elevation of 700 m asl (Neal et al. 1992). This local meteoric line ( $\delta D = 7.9 \pm 0.4 \delta^{18}O + 10.0 \pm 3.2$ ,  $n = 29$ ,  $r^2 = 0.93$ ) assumes a d-excess enrichment such as that of the mean Mediterranean Meteoric Water Line ( $\delta D = 8 \delta^{18}O + 15$ ) defined by Lambán and Custodio (1999). Indeed, d-excess values of these samples lie in the range between 12 and 18‰, which is also close to the range defined by Plata Bedmar (1994) for the groundwater isotopic content in Iberian Mediterranean basins, and consistent with the mentioned meteoric lines. Altitudinal isotopic gradients defined at nearby areas (Montseny range; Carmona et al. 2000; and eastern Pyrenees; Brusi et al. 2011) indicate that isotopic contents are consistent with the Sant Llorenç del Munt elevations, and that the variation of 1‰  $\delta^{18}O$  rightly covers the altitudinal difference existing between the summit and the surrounding valleys.

Most of the wells have their stable isotopic values arranged along a line of slope of 5 and an approximate origin at  $\delta^{18}O = -8.2\text{‰}$ ,  $\delta D = -50\text{‰}$ . This fact indicates that deep groundwater within the massif, pertaining to longer transit times flowlines, has undergone some evaporation processes that have enriched their isotopic water content. Only three

springs show a similar tendency. Given the geological setup of the SLMS, it can be conceived that springs respond to local, perched aquifer systems at distinct altitudes with a short residence time within the system. Indeed, the alluvial fan formation can be understood as a stratigraphically and tectonically compartmentalized system (Llopis 1944; Andrés 1964; Freixes 1986), as already deduced from the pumping tests. Contrarily, wells of hundreds of meters depth are recharged by a large-scale regional system that, due to the local orography, presents a thick unsaturated zone of hundreds of meters from the land surface to the water table. It is therefore reasonable to assume that some evaporation may occur during rainfall subsurface percolation along the fractures towards the water table. Deviation from the meteoric water line cannot be attributed to geographical effects such as continentality, since the distance between the closest and further points from the Mediterranean Sea is just 10 km.

According to Gonfiantini (1986) equations, the most evaporated groundwater sample (that is, from well S.LL-30) shows an evaporation percentage around 5%, assuming an isotopic composition of the atmospheric vapor of  $\delta^{18}O = -12\text{‰}$ ,  $\delta D = -86\text{‰}$ , and an observed mean daily relative humidity of  $70.0 \pm 0.2\%$  (Rellinars Observatory 2007–2017; RURALCAT 2017). Even though the displacement from the meteoric line shown by evaporated samples seems dramatic



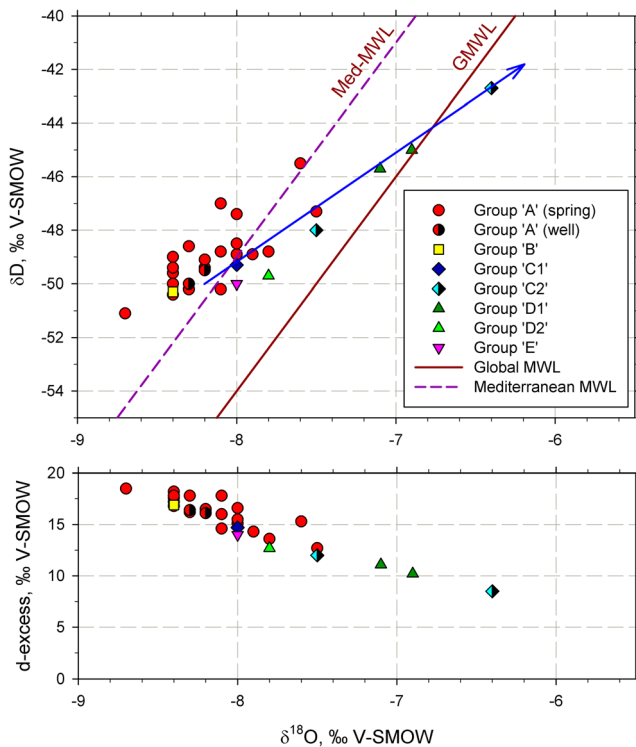


**Fig. 12** Relationship  $\delta D/\delta^{18}O$  for the summer 2011 field campaign, with representation of the Global and Mediterranean Meteoric Water Lines (GMWL and Med-MWL). The blue arrow represents a potential evaporation trend with an approximate origin at  $\delta^{18}O = -8.2\text{‰}$ ,  $\delta D = -50\text{‰}$ . Unless indicated (as for group A), the samples came from wells

when plotted as in Fig. 12, it only stands for a small percentage of water loss through evaporation in the unsaturated zone, even though this 5% loss represents a large volume of water at a regional scale. Although this is quantitatively inconsequential, it supports the interpretation of two distinct hydrogeological systems within the SLMS from a conceptual perspective: (1) a local one represented by spring data (mainly group A), which has not undergone isotopic fractionation, determined by the compartmentation of the main aquifers by fractures and low-permeability layers, and (2) a regional system that includes the general recharge all over the mountain range. This regional system recharges the deepest aquifer layers by downward percolation through a thick unsaturated zone. The good alignment of well isotopic data along an evaporation trend line assumes that groundwater is largely homogenized during the infiltration process. The role of distinct fracture systems with different hydraulic behaviors as double porosity, as also observed from field outcrops, contributes to the homogenization of the infiltrating recharge reflected by the isotopic data.

The sample from geochemical group E does not show any evaporation trend, suggesting a complex (mixed) circulation flow (see Fig. 13). Its sodium-bicarbonate facies would be caused by water–rock interaction processes occurring within

the delta front environment (Sg and Mgb). This geochemical group is based on data from a single well, so complementary data could provide further information.

## Discussion and conceptual flow model

Geological information compiled in the Sant Llorenç del Munt massif (Fig. 4) permits a comprehensive three-dimensional (3D) understanding of the lateral and vertical relationships among the 10 rock types. Lithofacies characteristics and diversity originated as a result of sediment accumulation in each part of the alluvial fan system. Further diagenetic processes will define the degree of compaction and cementation according to their original textural features. Such intrinsic primary sedimentological features, altogether with fracturation pattern (Alsaker et al. 1996), determine the Sant Llorenç de Munt hydrogeological system's final structure—that is, the occurrence of distinct hydrogeologic compartments at different scales. Stratigraphic and tectonic elements—namely, lithology, layer geometry and its lateral continuity, tilting and fracturing—become the key features that govern groundwater flow at the SLMS, configuring a compartmental system with two main hydrological dynamics.

Geomorphological evolution widens fracture apertures near the surface due to decompression and weathering, which will also be less intensive with depth. This implies that aquifer transmissivity will decrease with depth. Therefore, structural factors define the geometry of the aquifers within the SLMS as well as its hydraulic parameters (transmissivity and storativity). Indeed, pumping test analysis has pointed out the occurrence of impervious boundaries and the occurrence of different porosities (Fig. 6) in the flow system associated with the depositional units (specially, those with low hydraulic conductivity levels) and to the tectonic features of this mountain massif.

Hydrochemical and isotopic data provide an explanation of the groundwater flow path and of the relative transit times within the SLMS. Different hydrochemical facies illustrate the hydrochemical sequence that takes place within the system (Table 3). In general, most of the natural springs (group A) and a few wells present low EC and bicarbonate-calcium facies, which are indicative of low transit times within the system. Other groups show larger proportions of Mg, Na, Cl and  $SO_4$  that are attributed to the effect of groundwater flowpaths through distinct stratigraphic formations, as suggested by Mg occurrence and distribution. Indeed, Mg and  $SO_4$  enrichment indicate the influence of dolomite dissolution, whereas Na enrichment is caused by cationic exchange (Fig. 10) in clay-rich strata. Given the geological mapping and cross-sections of the area, hydrochemical facies of the well samples are fully justified by the predominant rock type around the borehole and along the regional flow-paths (Fig. 13).

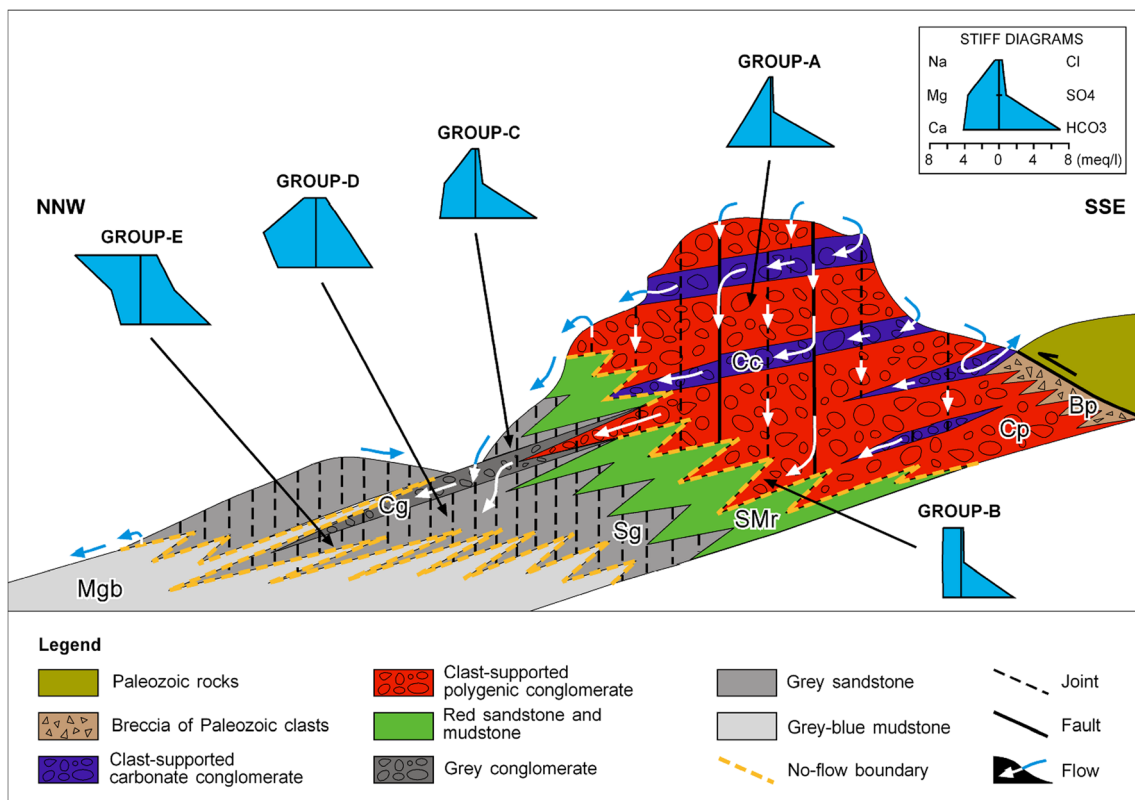


**Fig. 13** Conceptual hydrogeological model for the SLMS and evolutionary relationships among the different hydrochemical groups. Mountains to the *right* represent the main recharge area. Geology has

been simplified to show the hydrogeochemical evolution from the conglomerate units towards other lithological formations that modify groundwater composition due to water–rock interactions

In this sense, meteoric water recharge would be characterized as a group A facies in the initial reach of the downward groundwater flow path. Infiltration through conglomerates mainly generates a bicarbonate-calcium facies, constituting a local hydrological system. As groundwater flows within the system, it becomes enriched in Mg, Cl and/or Na, such as samples of B group, which represents a more evolved water within the alluvial fan area. Moreover, red sandstones and mudstones (SMr), which are laterally between conglomerates (Cp, Cc) and gray sandstones (Sg) layers, act as a low-permeability boundary, impeding groups A and B waters from continuing their flow towards the Sg sandstones and other down-gradient locations.

Infiltration through megajoints is facilitated by the fracture network which also allows hydraulic connection across low-permeability layers. Eventually, bicarbonate-calcium groundwater (group A) flows from alluvial fan conglomerates (Cp and Cc types) to delta front conglomerates and sandstones (Cg and Sg types, respectively), generating a second large-scale system. This happens basically in the upper part of the maximum progradation episodes (see preceding), resulting in an enrichment of Mg, SO<sub>4</sub>, Na and Cl (groups C and D types), and a depletion in Ca due to cation exchange processes, that finally defines group E groundwater samples. Therefore, flow towards the Sg formations is due to the fracture network and

some lateral progression of the Cp to Cg types that overcome the low hydraulic conductivity unit represented by SMr layers (Fig. 13). Recharge of the gray sandstone (Sg formation) also occurs by surface water infiltration.

From a hydrochemical perspective, surface water attains (partial) equilibrium with atmospheric conditions, and this may result in a loss of bicarbonate when it infiltrates and mixes with groundwater (group D). Resulting water undergoes further equilibration with the Sg formation lithology through water–rock interaction. Indeed, stream recharge is reinforced in some locations near Talamanca by small dams built to retain water and enhance infiltration.

Isotopic data support the described hydrochemical evolution. Groups A and B samples, which include all natural springs and a few wells, show a small isotopic variability that may just represent the altitude range of the recharges areas in the SLMS. Hydrochemical and isotopic similarity of all natural springs suggest a fast transit time within the system. The compartmentalized nature of the aquifer system defines mesh-type hydrogeological units limited by sedimentary discontinuities such as fine-sediment strata, and fractures. Given the thick conglomeratic units where they appear, the distinct sets of fractures are visibly responsible for controlling such local flow fields that discharge in natural springs. Locally, fracture flow may also discharge to eroding streams contributing to

surface runoff as baseflow. Isotopic data from deep wells, represented by hydrochemical groups C and D, show a clear evaporation trend which has been interpreted to be the result of a long pathway through the unsaturated zone and/or fracture systems before reaching the water table within the mountain range. Such recharge gets homogenized during its downward flow path as suggested by the allocation of the isotopic data along a single evaporation line. To some extent, the evaporation features of group C samples could also be attributed to some temporary subaerial conditions, yet it is plausible that most of the evaporation (up to 5%) takes place in the unsaturated zone because it implies a longer residence time than the atmospheric exposure.

The hydrochemical enrichment of major ions, as mentioned for these groups, does not occur in the unsaturated zone. Instead, it takes place within the main conglomeratic fractured aquifer that occupies the central part of the SLMS (Cp and Cc formations), and within the delta front lithologies (Cg and Sg formations) as the flowpath advances. In other words, the final hydrochemical content of samples from deep wells is acquired in the central part of the SLMS, homogenized across the unsaturated zone, and completed within the aquifer, below the water table, in equilibrium with the dominant lithology. Dissolution of Mg-rich minerals, pyrite oxidation, clay weathering, and cation exchange have been identified as the processes that contribute to their final hydrochemical features. Transitory surface flow and its later reinfiltration to the aquifer modifies the hydrochemical composition of some groundwater samples (group D), specially the carbonate system; although the final composition is clearly related to the hosting rock.

In the distal part of the alluvial fan, mudstone units embedded in the red sandstones (SMr) are the origin of layers with low hydraulic conductivity, especially the gray-blue mudstone unit (Mgb). In addition to the low permeability of these fine sediment layers, fractures (interjoints) in sandstone are not hydraulically effective since they do not propagate through the more plastic mudstone layers. Locally, the basinward displacement of the sedimentary facies belt at the time of maximum progradation occasionally permitted the sedimentation of conglomerates (Cg) in the marine zones which hydraulically connect the alluvial conglomerates (Cp, Cc) with the marine conglomerates and sandstones (Cg, Sg), providing an effective pathway for groundwater flow—an example of such a connection is found in well S.LL-27, whose discharge is significantly dependent on one of the conglomerate Cg layers deposited during a maximum progradation episode (Fig. 4).

More importantly, the distal evolution of Sg sandstones to Mgb mudstones, as well as the interfingering of both rock types, creates an important permeability barrier. This low-permeability boundary, assumed as impervious in a simple conceptual hydrogeological model, impedes groundwater flow further towards the NW, according to the main flow

direction controlled by the layer tilting. Such an impervious depositional boundary acts as a no-flow boundary and it determines the hydraulic head inside the entire SLMS and, consequently, the groundwater storage of the system (Fig. 13).

## Conclusions

The hydrogeological study of the Sant Llorenç de Munt alluvial fan system highlights the relevance of detailed geological knowledge in the understanding of groundwater dynamics in this mountain area. In this study, stratigraphical, sedimentological and tectonic data have provided the necessary information to build up a geological scheme that explains recharge processes and flow paths. The key geological features needed to understand groundwater paths within the system are vertical and lateral sedimentary variability (sedimentary architecture) and specifically the occurrence of low hydraulic conductivity units and no-flow limits, shown by the fracture pattern analysis. In this study case, head levels provide limited fragmentary information because of the lack of monitoring boreholes in the inner part of the massif and the occurrence of perched aquifers favored by stratigraphic and tectonic features. Pumping tests have also contributed to the understanding of the system. In addition to the hydraulic parameters, drawdown data provide information about the response of the system under exploitation and recharge. Identifying the occurrence of no-flow boundaries, as in the S.LL-27 deep well test, and double porosity within the aquifer layers, contributes to identifying the main aquifer geological features that govern groundwater flow, and to determining the extent of its potential exploitation.

Natural springs and their associated hydrochemical and isotopic data are highly valuable when trying to understand the dynamics of the system. On one hand, isotopic data reveal a compartmentalized system that recharges and drains groundwater via the separate flow subsystems that originate such springs. On the other hand, they also point out that a significant recharge occurs through a thick unsaturated zone within the massif (according to the evaporation isotopic evidence found in the deepest wells in contrast to that of natural springs). Furthermore, different hydrochemical facies can be clearly defined according to the water chemical equilibrium with the distinct lithology of each sedimentary unit.

Geological information validates the definition, first, of local-scale flow systems which result in natural springs; that is, those that flow through compartments or blocks limited by sedimentary facies changes and fractures. Secondly, it also defines a large regional flow system that controls the overall regional groundwater flow to lateral formations and is constrained finally by low-permeability units.

This kind of study of geological formations such as the Sant Llorenç de Munt mountain area where the stratigraphical

and tectonic structure outcrops and allows for observation of its geological features, provides a valuable scheme to be used as reference for groundwater-resources exploitation in similar buried systems elsewhere. Despite the fracture pattern being important for aquifer connectivity in lithified alluvial systems, fracturing should not be expected in unconsolidated fans (i.e., in recent, not lithified formations). Nevertheless, the flow field will be controlled by the characteristics of the sedimentary sequences (geometry, lithology, internal structure, etc.). In this context, hydrochemical and isotopic data stand as a complementary and predictive tool to unveil flow characteristics even where limited logging and geological information is available.

**Acknowledgements** We thank the water management companies in the area for their collaboration: Aigües de Manresa, Aigües de Terrassa and Sorea. We acknowledge the support provided by the municipalities of Mura, Talamanca, Pont Vilomara and Rocafort. We would like to thank the contribution of the “Catalana de Perforacions” and “Elèctrica Pintó” who provided borehole logs and pumping test data, as well as inputs from owners and managers of several privately owned springs. We are also thankful for the valuable comments made by the reviewers and the editor Dr. Elizabeth Sreaton. This research was partially funded by Spanish Government project CGL2013-48869-C2-2-R and CGL2011-29975-c04-04, which continues under project CGL2014-57215-C4-2-R.

## References

- Alsaker E, Gabrielsen RH, Roca E (1996) The significance of the fracture pattern of the late-Eocene Montserrat fan-delta, Catalan coastal ranges (NE Spain). *Tectonophysics* 266:465–491
- Anadón P (1978) El Paleogeno continental anterior a la transgresión Biarriztiense (Eoceno medio) entre los ríos Gaià y Ripoll (Provincias de Tarragona y Barcelona) [The continental Paleogene prior to the Biarrizian transgression (middle Eocene) between the Gaià and Ripoll rivers (Provinces of Tarragona and Barcelona)]. PhD Thesis, Facultat de Geologia, Universitat de Barcelona, Spain
- Anadón P, Cabrera L, Guimerà J, Santanach P (1985a) Paleogene strike-slip deformation and sedimentation along the southeastern margin of the Ebro Basin. In: Biddle KT and Christie-Blick N (eds) Strike-slip deformation, basin formation and sedimentation. *SEPM Spec Publ* 37:303–318
- Anadón P, Marzo M, Puigdefàbregas C (1985b) The Eocene fan delta of Montserrat (southeastern Ebro Basin, Spain). *Excursion 3, Field trip guidebook*, 6th European Regional Meeting I.A.S., Lleida, Spain, April 1985
- Anders R, Mendez GO, Futa K, Danskin WR (2014) A geochemical approach to determine sources and movement of saline groundwater in a coastal aquifer. *Ground Water* 52(5):756–768
- Andrés O (1964) Karstificación en conglomerados. Su estudio en el macizo de Sant Llorenç del Munt - serra de l'Obac (Barcelona) [Karstification in conglomerates: his study in the massif of Sant Llorenç del Munt - Serra de l'Obac (Barcelona)]. *Geo y Bio Karst* 2:9–12
- Anglés M (2013) Hidrostratigrafia del ventall deltaic de Sant Llorenç del Munt (Eocè mig-superior, Conca de l'Ebre) [Hydrostratigraphy of the Sant Llorenç del Munt fan delta (middle-upper Eocene, Ebro Basin)]. PhD Thesis, Universitat Autònoma de Barcelona, Spain
- Anglés M, Maestro E (2010–2011) Els conglomerats de Sant Llorenç del Munt (Eocè mitjà-superior) [Sant Llorenç del Munt conglomerates (middle-upper Eocene)]. *Bull Instít Catalana Història Nat* 76: 71–82
- Arenas C, Millán H, Pardo G, Pocoví A (2001) Ebro Basin continental sedimentation associated with late compressional Pyrenean tectonics (north-eastern Iberia): controls on basin margin fans and fluvial systems. *Basin Res* 13:65–89
- Benvenuti M (2003) Facies analysis and tectonic significance of lacustrine fan-deltaic successions in the Pliocene-Pleistocene Mugello Basin, central Italy. *Sediment Geol* 157:197–234
- Blair TC (2000) Sedimentology and progressive tectonic unconformities of the sheetflood-dominated Hell's gate alluvial fan, Death Valley, California. *Sediment Geol* 132:233–262
- Brusi D, Ramonell C, Menció A, Roqué C, Mas-Pla J (2011) Isotopic characterization of ground water in western Pyrenees. 9th Int. Symposium on applied geochemistry. Tarragona, Spain, September 2011, Abstracts
- Cabello P, Falivene O, López-Blanco M, Howell J, Arbués P, Ramos E (2011) An outcrop-based comparison of facies modelling strategies in fan-delta reservoir analogues from the Eocene Sant Llorenç del Munt fan-delta (NE Spain). *Pet Geosci* 17:65–90
- Carmona JM, Bitzerb K, López E, Bouazza M (2000) Isotopic composition and origin of geothermal waters at Caldetes (Maresme-Barcelona). *J Geochem Explor* 69–70:441–447
- Carrillo-Rivera JJ, Irén Varsányi I, Kovács LO, Cardona A (2007) Tracing groundwater flow systems with hydrogeochemistry in contrasting geological environments. *Water Air Soil Pollut* 184:77–103
- Chapius RP (1994) Assessment of methods and conditions to locate boundaries: I. one or two straight impervious boundaries. *Groundwater* 32(4):576–582
- Chen W-F, Liu T-K (2003) Dissolved oxygen and nitrate of groundwater in Choshui Fan-Delta, western Taiwan. *Environ Geol* 44:731–737
- Chen W-F, Liu T-K (2005) Ion activity products of iron sulphides in groundwaters: implications from the Choshui fan-delta, western Taiwan. *Geochim Cosmochim Acta* 69(14):3535–3544
- Craig H (1961) Isotopic variations in meteoric waters. *Science* 133:1702–1703
- DeCelles PG, Gray MB, Ridgway KD, Cole RB, Pivnik DA, Pequera N, Srivastava P (1991) Controls on synorogenic alluvial-fan architecture, Beartooth conglomerate (Palaeocene), Wyoming and Montana. *Sedimentology* 38:567–590
- Epstein S, Mayeda T (1953) Variation of O<sup>18</sup> content of waters from natural sources. *Geochim Cosmochim Acta* 4(5):213–224
- Folch A, Menció A, Puig R, Soler A, Mas-Pla J (2011) Groundwater development effects on different scale hydrogeological systems using head, hydrochemical and isotopic data and implications for water resources management: the Selva basin (NE Spain). *J Hydrol* 403(1–2):83–102
- Freixes A (1986) El carst conglomeràtic experimental de Rellinars: un enfocament sistèmic i hidrogeològic en la recerca del medi càrstic [The experimental conglomeratic karst of Rellinars: a systemic and hydrogeological approach in the karst environment research]. Research Project, Facultat de Geologia, Universitat de Barcelona, Spain
- Galloway WE, Hobday DK (1996) Terrigenous clastic depositional systems: applications to fossil fuel and groundwater resources, 2nd edn. Springer, Heidelberg, Germany
- Gonfiantini R (1986) Environmental isotopes in lake studies. In: Fritz P, Fontes JCh (eds) *Handbook of environmental isotope geochemistry*, vol 2. Elsevier, Amsterdam, pp 113–168
- Grau A, Castells R, Deu M, Guàrdia A, Guerrero C, Roijals X, Burriel JA, Ibàñez JJ, Pons X (2007) El mapa de cobertes del sòl de Catalunya com a eina d'estudi de Sant Llorenç del Munt i l'Obac [The soil cover map of Catalonia as a tool to study Sant Llorenç del Munt i l'Obac]. VI Trobada d'Estudiosos de Sant Llorenç del Munt i l'Obac. Diputació de Barcelona, Barcelona, Spain
- Harvey AM, Mather AE, Stokes M (2005) Alluvial fans: geomorphology, sedimentology, dynamics: introduction—a review of alluvial-fan

- research. In: Harvey AM, Mather AE, Stokes M (eds) Alluvial fans: geomorphology, sedimentology, dynamics. Geol Soc Lond Spec Publ 251:1–7
- ICGC (2003) Mapa Geològic de Catalunya 1:25.000, Full 392-1-1 (71–29) Monistrol de Montserrat [Geological map of Catalonia 1:25,000, Sheet 392-1-1 (71–29) Monistrol de Montserrat]. Institut Cartogràfic i Geològic de Catalunya, Barcelona
- ICGC (2010) Mapa geològic de Catalunya, Geotrell I, Mapa geològic 1:25.000 - Full 363-2-2 (72–28) Sant Llorenç Savall [Geological map of Catalonia, Geowork I, Geological map 1:25,000 – Sheet 363-2-2 (72–28) Sant Llorenç Savall]. Institut Cartogràfic i Geològic de Catalunya, Barcelona
- ICGC (2011a) Mapa geològic de Catalunya, Geotrell I, Mapa geològic 1:25.000 - Full 392-2-1 (72–29) Castellar del Vallès [Geological map of Catalonia, Geowork I, Geological map 1:25,000 – Sheet 392-2-1 (72–29) Castellar del Vallès]. Institut Cartogràfic i Geològic de Catalunya, Barcelona
- ICGC (2011b) Mapa geològic de Catalunya, Geotrell I, Mapa geològic 1:25.000 - Full 363-1-2 (71–28) Manresa [Geological map of Catalonia, Geowork I, Geological map 1:25,000 – Sheet 363-1-2 (71–28) Manresa]. Institut Cartogràfic i Geològic de Catalunya, Barcelona
- IDESCAT (2016) El municipi en xifres [The municipality in figures]. Institut d'Estadística de Catalunya. <http://www.idwvscat.cat/emex>. Accessed 16 February 2017
- Lambán J, Custodio E (1999) Estudio isotópico ambiental ( $O^{18}$ -D) en la Unidad Anoia: Principales zonas de recarga e implicaciones en el funcionamiento hidrogeológico del Sistema [Environmental isotopic study ( $O^{18}$ -D) in the Anoia unit: main recharge zones and implications in the hydrogeological operation of the system]. Ing Agua 6(2):139–150
- Li J, Li F, Liu Q, Zhang Y (2014) Trace metal in surface water and groundwater and its transfer in a Yellow River alluvial fan: evidence from isotopes and hydrochemistry. Sci Total Environ 472:979–988. doi:10.1016/j.scitotenv.2013.11.120
- Lindholm RC, Finkelman RB (1972) Calcite staining: semiquantitative determination of ferrous iron. J Sediment Res 42(1):239–242
- Llopis N (1944) Morfoestructura de los relieves de pudingas de Sant Llorenç del Munt - serra de l'Obac (Barcelona) [Morphostructure of the conglomeratic reliefs of Sant Llorenç del Munt - Serra de l'Obac (Barcelona)]. Estud Geogràf 17:687–814
- López-Blanco M (1994) Estructuras contractivas de la cordillera Prelitoral Catalana entre la sierra de les Pedritxes y el río Ripoll: evolución y relación con los depósitos del margen de la cuenca del Ebro [Contractive structures of the Catalan coastal ranges between the les Pedritxes Mountain range and the Ripoll River: evolution and relation with the deposits of the Ebro Basin margin]. Geogaceta 16: 43–46
- López-Blanco M (1996) Estratigrafia secuencial de sistemas deltaicos en cuencas de antepaís: ejemplos de Sant Llorenç del Munt, Montserrat y Roda (Paleógeno, cuenca de antepaís surpireanica) [Sequence stratigraphy of deltaic systems in foreland basins: examples of Sant Llorenç del Munt, Montserrat and Roda (Paleogene, South-Pyrenean Foreland Basin)]. PhD Thesis, Universitat de Barcelona, Spain, 238 pp
- López-Blanco M (2006) Stratigraphic and tectosedimentary development of the Eocene Sant Llorenç del Munt and Montserrat fan-delta complexes (Southeast Ebro basin margin, Northeast Spain). Contrib Sci 3(2):125–148
- Maestro E (1987) Estratigrafia i fàcies del complex deltaic (Fan delta) de Sant Llorenç del Munt (Eocè mig-superior, Catalunya). [Stratigraphy and facies of the deltaic complex (fan delta) of Sant Llorenç del Munt (middle-upper Eocene, Catalonia)]. PhD Thesis, Facultat de Ciències, Universitat Autònoma de Barcelona, Bellaterra, Spain
- Mas-Pla J, Bach J, Viñals E, Trilla J, Estalrich J (1999) Salinization processes in a coastal leaky aquifer (alt Empordà, NE Spain). Phys Chem Earth Part B 24(4):337–341
- Mas-Pla J, Menció A, Bach J, Soler D, Zamorano M, Brusi D (2016) Trace element groundwater pollution hazard in regional hydrogeological systems (Empordà basin, NE Spain). Water Soil Air Pollut 227:218–240
- Mata-Perelló JM (1990) Els minerals de Catalunya [The Catalonia minerals]. Institut d'Estudis Catalans, Barcelona, Spain, 441 pp
- Menció A, Mas-Pla J, Otero N, Regàs O, Boy-Roura M, Puig R, Bach J, Domènech C, Zamorano M, Brusi D, Folch A (2016) Nitrate pollution of groundwater: all right ..., but nothing else? Sci Total Environ 539C:241–251
- Neal C, Neal M, Warrington A, Avila A, Pinol J, Roda F (1992) Stable hydrogen and oxygen isotope studies of rainfall and streamwaters for two contrasting holm oak areas of Catalonia, northeastern Spain. J Hydrol 140:163–178
- Otero N, Canals A, Soler A (2007) Using dual-isotope data to trace the origin and processes of dissolved sulphate: a case study in Calders stream (Llobregat basin, Spain). Aquatic Geochem 13:109–126
- Peng T-R, Lu W-C, Chen K-Y, Zhan W-J, Liu T-K (2014) Groundwater-recharge connectivity between hills-and-plains area of western Taiwan using water isotopes and electrical conductivity. J Hydrol 517:226–235
- Plata Bedmar A (1994) Composición isotópica de las aguas subterráneas de la Península Ibérica [Isotopic composition of the Iberian Peninsula groundwater]. Pub. M-39, Centro de Estudios y Experimentación de Obras Públicas, Madrid
- Renard P, Glenz D, Mejias M (2009) Understanding diagnostic plots for well-test interpretation. Hydrogeol J 17(3):589–600
- RURALCAT (2017) Dades meteorològiques: la comunitat virtual agroalimentària i del món rural [Meteorological data: the virtual community agro-food and of the rural world]. Generalitat de Catalunya. <http://www.ruralcat.net/web/guest/reg.dadesmeteo>. Accessed 16 February 2017
- Sohn YK, Rhee CW, Kim BC (1999) Debris flow and hyperconcentrated flood-flow deposits in an alluvial fan, northwestern part of the cretaceous Yongdong Basin, central Korea. J Geol 107:111–132
- Tóth J (1995) Hydraulic continuity in large sedimentary basins. Hydrogeol J 3:4–16
- Tóth J (2000) Las aguas subterráneas como agente geológico: causas, procesos y manifestaciones [Groundwater as a geological agent: causes, processes and manifestations]. Bol Geol Min 111(4):9–26
- Tsang CF, McEdwards DG, Narashiman TN, Witherspoon PA (1977) Variable flow well-test analysis by a computer-assisted matching procedure. Paper no. 6547, 47th Annual Western Regional Meeting, SPE of AIME, Bakersfield, CA, April 1977
- Yechieli Y, Shalev E, Wollman S, Kiro Y, Kafri U (2010) Response of the Mediterranean and Dead Sea coastal aquifers to sea level variations. Water Resour Res 46:1–11